

DISCOVERY OF A LARGE POPULATION OF ULTRALUMINOUS X-RAY SOURCES IN THE BULGE-LESS GALAXIES NGC 337 AND ESO 501-23

GARRETT SOMERS¹, SMITA MATHUR^{1,2}, PAUL MARTINI^{1,2}, LINDA WATSON³, CATHERINE J. GRIER¹ AND LAURA FERRARESE⁴
Draft version October 17, 2018

ABSTRACT

We have used *Chandra* observations of eight bulge-less disk galaxies to identify new ultraluminous X-ray source (ULX) candidates, study their high mass X-ray binary (HMXB) population, and search for low-luminosity active galactic nuclei (AGN). We report the discovery of 16 new ULX candidates in our sample of galaxies. Eight of these are found in the star forming galaxy NGC 337, none of which are expected to be background contaminants. The HMXB luminosity function of NGC 337 implies a star formation rate (SFR) of $6.8_{-3.5}^{+4.4} \text{ M}_\odot \text{ yr}^{-1}$, consistent at 1.5σ with a recent state of the art SFR determination. We also report the discovery of a bright ULX candidate (X-1) in ESO 501-23. X-1's spectrum is well fit by an absorbed power law with $\Gamma = 1.18_{-0.11}^{+0.19}$ and $N_{\text{H}} = 1.13_{-1.13}^{+7.07} \times 10^{20} \text{ cm}^{-2}$, implying a 0.3-8 keV flux of $1.08_{-0.07}^{+0.05} \times 10^{-12} \text{ erg s}^{-1} \text{ cm}^{-2}$. Its X-ray luminosity (L_X) is poorly constrained due to uncertainties in the host galaxy's distance, but we argue that its spectrum implies $L_X > 10^{40} \text{ erg s}^{-1}$. An optical counterpart to this object may be present in HST imaging. We also identify ULX candidates in IC 1291, PGC 3853, NGC 5964 and NGC 2805. We find no evidence of nuclear activity in the galaxies in our sample, placing a flux upper limit of $4 \times 10^{-15} \text{ erg s}^{-1} \text{ cm}^{-2}$ on putative AGN. Additionally, the type II-P supernova SN 2011DQ in NGC 337, which exploded 2 months before our X-ray observation, is undetected.

Subject headings: galaxies: nuclei – galaxies: bulge-less – X-rays: galaxies – X-rays: binaries

1. INTRODUCTION

Ultraluminous X-ray sources (ULXs) are extra-Galactic, off-nuclear X-ray objects which radiate at $\gtrsim 2 \times 10^{39} \text{ erg s}^{-1}$ in the 0.3-10 keV range, assuming isotropic emission (for a recent review, see Feng & Soria 2011). This is a remarkable luminosity, as it represents the Eddington limit for an accretion disk around the most massive stellar mass black holes (StMBHs) known in the Galaxy ($\sim 20 \text{ M}_\odot$; e.g. Remillard & McClintock 2006). Over one hundred ULX candidates have now been identified in the local universe (Winter et al. 2006, Swartz et al. 2011), though the number with well-sampled spectra remains low. The most natural explanation for these objects are accreting black holes with masses in the range $10^2 - 10^5 \text{ M}_\odot$, often referred to as intermediate mass black holes (IMBHs; Colbert & Mushotzky 1999). This explanation gained popularity because it does not violate the Eddington limit, and explains ULXs in the well known framework of black hole binaries. Indeed, early investigations of ULXs found evidence of cool accretion disks and, in some cases, quasi-periodic oscillations (QPOs) in their spectra, both indicative of IMBH binaries (see Miller & Colbert 2004 for a review). In particular, the object ESO 243-49 HLX-1 is one of the strongest known IMBH candidates (Farrell et al. 2009). However, recent arguments, such as the unphysically large amount of mass required to reproduce the ULX populations in

some galaxies (King et al. 2004, see also Roberts 2007), have disfavored the theory that IMBHs dominate the ULX population. Other authors have suggested strong beaming from sub-Eddington accretion onto a StMBH (e.g. King et al. 2001), although the discovery of emission nebulae around several ULXs argues for mostly isotropic emission (Pakull & Mirioni 2003).

An alternative explanation for ULXs involves super-Eddington accretion onto a stellar mass black hole, perhaps with mild beaming (e.g. King et al. 2001, Begelman 2002). This requires a different accretion paradigm than the classic thin disk models (Shakura & Sunyaev 1973), such as the class of optically thick, slim disk models (e.g. Abramowicz et al. 1988, Watari 2000, Poutanen et al. 2007), which can radiate at several times Eddington. This may result in a previously unknown black hole binary (BHB) accretion state dubbed the ultraluminous state (Gladstone et al. 2009) which may characterize StMBH binaries for a fraction of their lifetime. In this frame work, ULXs would represent the high-mass end of the high mass X-ray binary (HMXB) distribution, radiating in their most extreme state. This idea is supported by the discovery of luminous blue stellar counterparts to several ULXs, a necessary component of a HMXB (Liu et al. 2004, Levan & Goad 2008, Jonker et al. 2012). Furthermore, ULXs are preferentially found in regions of recent star formation and low metallicity (Kaaret 2005, Swartz et al. 2009, Pakull & Mirioni 2002), likely nurseries of massive StMBHs and binary companions (Belczynski et al. 2010). Only dynamical mass measurements can definitively confirm the nature of these mysterious objects, so for now the controversy persists.

If some ULXs contain IMBHs, their study may provide insight into the formation of super massive black holes (SMBH), which likely grow from intermediate mass

¹ Department of Astronomy, The Ohio State University, 140 W. 18th Ave, Columbus, OH 43210; somers@astronomy.ohio-state.edu

² Center for Cosmology and Astroparticle Physics, The Ohio State University, 191 W Woodruff Avenue, Columbus, OH 43210, USA

³ Harvard-Smithsonian Center for Astrophysics, 60 Garden Street, Cambridge, MA 02138, USA

⁴ Herzberg Institute of Astrophysics, 5071 West Saanich Road, Victoria, BC, V9E 2E7, Canada

seeds. The relationship between IMBHs and SMBHs is of great importance to the study of galaxy evolution, as observations of active galactic nuclei (AGN) and their host environments provide strong evidence that galaxies and their central black holes co-evolve. In particular, the $M_{\text{BH}}-\sigma_{\text{Bulge}}$ relationship and the $M_{\text{BH}}-M_{\text{Bulge}}$ relationship (Ferrarese & Merritt 2000, Gebhardt et al. 2000, Häring & Rix 2004) imply that the evolutionary history of a galaxy and its central massive black hole may be connected. Since these correlations are fundamental to our understanding of hierarchical galaxy formation and evolution in the Λ CDM universe (e.g. Menci et al. 2004), the full parameter space of M_{BH} , M_{Bulge} , and σ_{Bulge} must be explored. Although the $M_{\text{BH}}-\sigma_{\text{Bulge}}$ relation holds in many mass regimes, it should break down in bulge-less galaxies if the formation of a SMBH is connected to the presence of a bulge. Yet in some cases, SMBHs have been identified in bulge-less galaxies by their X-ray AGN signatures (Filippenko & Ho 2003, Satyapal et al. 2007, Shields et al. 2008, Ghosh 2009, Secretan et al. 2012, Araya Salvo et al. 2012). This has led some to hypothesize that SMBHs in late type galaxies are formed through different processes than black holes associated with spheroidal systems (Kormendy & Bender 2011). Bulge-less galaxies therefore provide a crucial laboratory for studying galaxy growth in a regime where our understanding of SMBH/galaxy co-evolution may differ from the standard model (Mathur et al. 2012). Although statistics about the prevalence of bulge-less AGN are beginning to accumulate, more late type galaxies must be observed to probe the low mass end of the $M_{\text{BH}}-\sigma_{\text{Bulge}}$ relation.

In this paper we discuss *Chandra* observations of eight nearby, late-type galaxies (see Table 1) selected from among the twenty objects studied in Watson et al. (2011, W11 hereafter). W11 conducted a survey in a variety of wavelengths to study the effects of rotation speed on star formation in bulge-less galaxies (see also Watson et al. 2012). In particular, their sample was selected to straddle the critical 120 km s⁻¹ rotation speed where the properties of the cold ISM appear to change abruptly (Dalcanton et al. 2004). From their set of twenty, we selected eight galaxies that span the full range of mass, star formation rate, and rotational velocity explored in their study. We report here our findings from the analysis of these observations. In §2, we briefly describe the *Chandra* observations and our reduction and analysis methods. §3 contains a description of the X-ray populations within each galaxy in the sample, and highlights potentially interesting sources. §4 presents the results of our search for nuclear activity, and describes the ULX candidate populations of NGC 337 and ESO 501-23. Finally, §5 summarizes our conclusions. Throughout this paper, we make use of the log N –log S formulation of Moretti, Campana, Lazzati and Tagliaferri (2003, M03 hereafter)⁵ as a rough estimate of the expected number of cosmic X-ray background (CXB) objects above a given flux limit.

2. OBSERVATIONS & DATA REDUCTION

⁵ For the soft band 0.5-2.0 keV, and the hard band 2.0-10.0 keV, the number of sources expected, per square degree, above flux limit S (cgs): $N_S(>S) = \frac{1.09 \times 10^{-23}}{S^{1.82} + 1.34 \times 10^{-17} S^{0.60}}$ and $N_H(>S) = \frac{4.43 \times 10^{-20}}{S^{1.57} + 6.14 \times 10^{-17} S^{0.44}}$.

The observations were undertaken with the *Chandra* X-ray Observatory (Weisskopf et al. 2000) Advanced CCD Imaging Spectrometer (ACIS) between November 2010 and January 2012. Each galaxy was imaged for 9.93 ks using the ACIS S-array chips S2 through S4, with the galaxy centered on the back illuminated S3 chip. Following the observations, *Chandra* X-ray FITS files were downloaded from the *Chandra Data Archive* and analyzed with the *Chandra* Interactive Analysis of Observations suite (CIAO; Fruscione et al. 2006) version 3.4. Following the method of Ghosh et al. (2008), we produced level 2 event files from the acquired level 1 event files by applying grade, status, and good time interval filters, and limiting our observations to the 0.3-8 keV range. We searched for contaminating background flares by binning the exposure of each chip into 30 time bins (~ 300 s each). If the count rate of a bin deviated from the mean by more than 10%, that bin was excluded from further analysis. The details of each observation, including the background flare-subtracted exposure times, are listed in Table 2.

Next, we used the CIAO task WAVDETECT on each chip to identify potential X-ray objects. At the location of each candidate, counts were extracted from a 95% energy enclosed circle, 2.3'' for on-axis point sources, and larger for off-axis point sources. The background contribution was removed using an annulus with an inner (outer) radius of 2 \times (5 \times) the source extraction circle's radius. For sources that lay on the edge of the CCD, a half annulus was used to determine the background and the effects of off-CCD dithering were taken into account. If another detected source fell within the annulus, it was excised before the count rate was determined. WAVDETECT sources with less than 5 counts, or with less than a 2 σ deviation above the background flux, were rejected. These criteria were chosen to ensure minimal false positives, which can be numerous in low signal-to-noise data. Absolute astrometric errors are less than 0.8'' for 99% of *Chandra* sources. We tested this by examining the relative astrometry of sources with obvious SDSS counterparts, and found that typical offsets were within this error.

3. X-RAY RESULTS

WAVDETECT identified a total of 190 candidate sources within our eight fields. Sixteen of these were discarded based on our rejection criteria, leaving the 174 objects listed in Table 3. These objects range in nature from background galaxies, to foreground stars, to X-ray binaries within the targeted galaxies. To identify potential counterparts to these sources, we cross correlated our sample with the USNO-B1.0, SDSS DR8, and WISE point source catalogs using the *Vizier*⁶ database (Monet et al. 2003, Adelman-McCarthy et al. 2011, Wright et al. 2010). Objects falling within 2'' of a source in Table 4 were included. *Chandra*'s 90% source location on-axis error circle is 0.6'', and 99% of all sources fall within 1'', so more distant objects are unlikely to be physically related. Nevertheless, we include them in our cross-correlation table to account for the larger positional error of off-axis sources, and the possibility of significant proper motion between epochs. The resulting source lists

⁶ <http://vizier.u-strasbg.fr/viz-bin/VizieR>

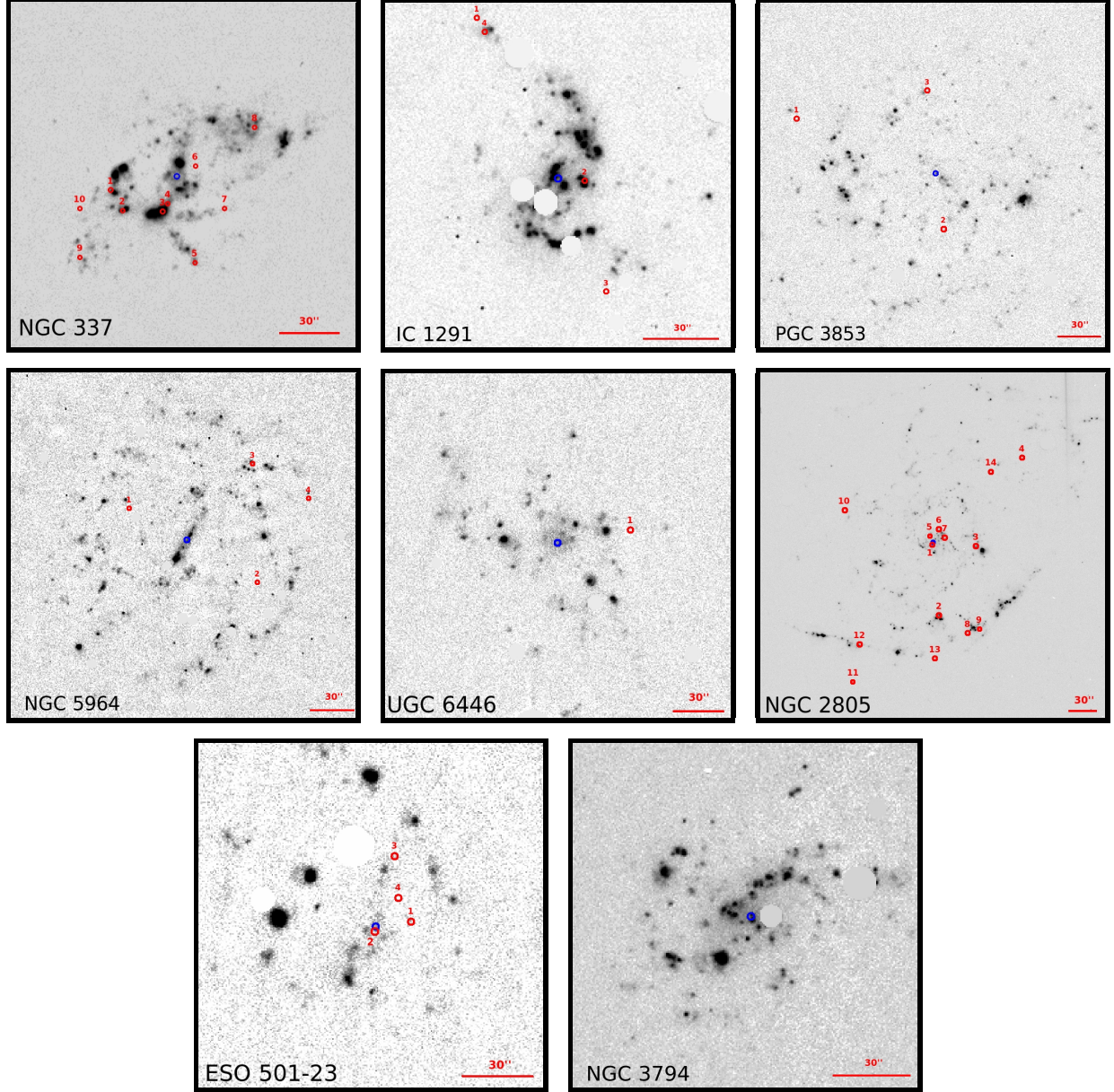


FIG. 1.— X-ray source locations (red points) from Table 7, superimposed on H α images (gray scale) from the 2.4m Hiltner Telescope at MDM Observatory (see W11 for details). Blue circles represent the central coordinates listed in Table 1.

are in Tables 4, 5, and 6.

Forty X-ray sources are detected within the combined 25th mag arcsec $^{-2}$ B-band isophotes (D25) of the eight galaxies in the sample (see Table 1), including 18 with fluxes consistent with ULXs. These sources are listed in Table 7. H α images of the galaxies are shown in Figure 1, over plotted with X-ray source locations. Due to the high probability of CXB contamination, each source must be evaluated individually to determine its nature. This is possible in some cases when the object is sufficiently bright, or when counterparts can be identified. We briefly describe the findings for each galaxy here, and highlight potentially interesting sources.

3.1. NGC 337

NGC 337 is an SBd galaxy at a distance of 20.7 Mpc (see Table 2). This object is part of the SINGS sample of galaxies (Kennicutt et al. 2003), and has been exten-

sively studied in the literature. Our exposure uncovered ten sources within the D25 ellipse, including eight whose fluxes are consistent with ULXs, as seen in Figure 1. M03 predict ~ 0.6 soft and ~ 1.3 hard background sources above our flux limit within this area, which implies the existence of a large population of ULXs associated with NGC 337. These objects will be examined further in §4.2. Additionally, this *Chandra* observation was taken ~ 2 months after the discovery of the type II-P supernova SN 2011DQ in NGC 337. This event was located at R.A. = $00^{\text{h}}59^{\text{m}}47.75^{\text{s}}$, Dec. = $07^{\text{d}}34^{\text{m}}20.5^{\text{s}}$ (J2000), and is clearly within the galactic disk (Barbon et al. 2009). No counts above the background rate were detected at this location, corresponding to a 3σ upper limit of 2.8×10^{38} erg s $^{-1}$ from 0.3–8 keV. This is not surprising: although several type II-P supernovae have been detected in X-rays, such as SN 2004dj (Pooley and Lewin 2004), their

X-ray luminosities at a distance of 20.7 Mpc would be below the detection limit at the time of our observation.

3.2. IC 1291

IC 1291 is an SBdm galaxy at a distance of 31.5 Mpc. We find four sources in this galaxy, two of which (X-1 and X-2) have fluxes consistent with ULXs at high significance ($> 3\sigma$), and two (X-3 and X-4) with moderate significance ($\sim 1\sigma$). X-1 and X-4 lie outside the D25 diameter listed in RC3, but within the D25 diameter listed in other catalogs (e.g. Tully 1988), so we include them in our table. H α observations imply that this galaxy is in an epoch of star formation, and thus is expected to host a few bright X-ray sources. X-2 is perhaps the best ULX candidate, as it coincides with a bright H α region and has a bright optical counterpart in HST images. However, due to the considerable distance of IC 1291 and the low signal-to-noise of our observation, only 28 net counts were observed for this object. Deeper exposures are therefore needed to confirm its nature. We caution that the two dimmer sources, despite being at the ULX flux level, are also consistent with CXB contaminants. This is because only 8.5 net counts are needed to infer a luminosity in excess of 10^{39} erg s $^{-1}$ at 31.5 Mpc, and M03 predict ~ 1 CXB source in this observation.

3.3. PGC 3853

PGC 3853 is an SABd galaxy at a distance of 11.4 Mpc. We find three sources in this galaxy, two that are dim (~ 5 cts) and one that is bright ($\gtrsim 150$ cts). M03 predict ~ 5 CXB sources in this observation, implying that some or all PGC 3853 detections may be contaminants. Using H α and HST images, we find no obvious optical counterparts to the dimmer sources, X-2 and X-3. Considering their low fluxes, we conclude they are likely distant background galaxies. X-1 is bright enough that it is likely associated with PGC 3853, but it does not lie in an area of recent star formation, and does not have any obvious optical counterparts in HST imaging or our cross-correlation tables. It is still possible that this source is a ULX, as Swartz et al. (2009) found that only $\sim 60\%$ of ULXs are associated with areas of recent star formation.

3.4. NGC 5964

NGC 5964 is an SBd galaxy at a distance of 24.7 Mpc. There are four sources within the D25 ellipse of this galaxy, two (X-3 and X-4) that are below the ULX threshold ($\lesssim 10$ cts), and two (X-1 and X-2) that are above ($\gtrsim 20$ cts). M03 predict ~ 5 CXB sources in this observation, and patchy H α emission implies an absence of large scale star formation in the recent past, so these sources are consistent with background contaminants. However, X-3 is relatively close to a region with a young stellar population, and might be associated with a black hole binary that has now traveled away from its birth location. The projected separation between the X-ray source and the nearby H α source is ~ 150 pc, and could be covered within a few 10s of Myrs at reasonable speeds. The two brightest sources, NGC 5964 X-1 and X-2, have no obvious visible counterparts or H α association, so their nature remains unclear.

3.5. UGC 6446

UGC 6446 is an SAd galaxy at a distance of 18.0 Mpc. Our exposure reveals one dim source within the D25 ellipse. We detect only 4.7 net counts, near our detection threshold but statistically significant. If this source is real, it could be a high-mass X-ray binary within UGC 6446 or, more likely, a background contaminant. As this galaxy is weak in H α , the lack of notable X-ray sources is not surprising.

3.6. NGC 2805

NGC 2805 is an SABd galaxy at a distance of 28.0 Mpc. This galaxy has the largest population of X-ray point sources in our sample, with fourteen detections inside D25 and five consistent with ULXs. It also has the largest projected area in our sample, and M03 predict twelve background sources above our detection limit, including five consistent with ULXs. Due to the large expected CXB contribution, it is difficult to draw conclusions about the X-ray population of this galaxy. However, we note that ten of the fourteen sources appear consistent with areas of recent star formation, a fraction that would be difficult to produce with randomly oriented background sources. Additionally, four of the sources lie within the central 15'' of the galaxy, another unlikely orientation for background sources. Finally, the H α measurements of W11, the H α /SFR relation of Kennicutt (1998), and the SFR/N($L > 2 \times 10^{38}$ erg s $^{-1}$) relation of Grimm, Gilfanov, and Sunyaev (2003, G03 hereafter) predict four X-ray sources above our flux limit within the D25 ellipse of NGC 2805. This implies that eleven of the sources are background, consistent with the prediction of M03. For these reasons, we conclude that several of these bright X-ray sources are likely associated with NGC 2805. X-3, X-4 and X-8 in particular are strongly consistent with ULXs, and are the best candidates in this observation.

3.7. ESO 501-23

ESO 501-23 is an SBdm galaxy at an adopted distance of 7.01 Mpc, although this distance is uncertain by a factor of two (see §4.3). We find a total of four objects within this galaxy, including the brightest X-ray source discovered in this survey, ESO 501-23 X-1. This object is discussed further in §4.3. The source X-2 lies only $\sim 2''$ from the galactic center listed in Table 2. However, because of the peculiar shape of this galaxy, there is significant disagreement about the location of the galactic center, and several independent determinations of the central coordinates exist, as shown in Figure 2. Therefore, we do not claim this object is an AGN, although this possibility should not be discarded given its proximity to the central region. We can identify X-3 as a nearby star seen in HST imaging, and recorded in the Carlsberg-Meridian Catalog (CMC 2006). X-4 has no identifiable optical or IR counterpart, so it may be a HMXB or a CXB source.

3.8. NGC 3794

NGC 3794 is an SABd galaxy at a distance of 19.2 Mpc. No *Chandra* sources were identified within the D25 ellipse of this galaxy, moderately consistent with the M03 prediction of ~ 1.3 sources above the flux limit.

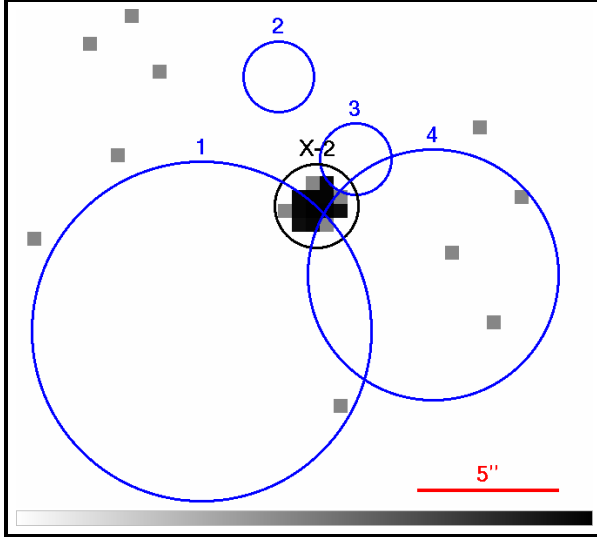


FIG. 2.— Unsmoothed image of ESO 501-23 X-2, shown with four reported central coordinates of the host galaxy. In order, #1 is from RC3 (de Vaucouleurs et al. 1991), #2 is from the HYPERLEDA catalog (Paturel et al. 2003), #3 is from the 6 degree field survey (Jones et al. 2005), and #4 is from W11. The first three are photometric centers, while the fourth is a dynamical center. The size of each circle represents the positional uncertainty of the determination. Up is North and left is East.

4. DISCUSSION

4.1. AGN Candidates

We searched the central regions of the eight galaxies for evidence of AGN activity. There is considerable difficulty in determining the central coordinates of bulge-less galaxies, which often lack an easily identifiable central structure. In particular, dynamical measurements of the central coordinates disagree with photometric measurements at the $\gtrsim 5''$ level for NGC 2805 and ESO 501-23. Inner and outer photocenters may differ as well. This makes AGN detection claims difficult, as sub-arcsecond confidence is required to confirm nuclear activity. In Table 1 we adopt photometric centers from 2MASS, SDSS and 6dF as the galactic central coordinates. AGN at these coordinates, as well as the kinematic centers determined by W11, with $f_{0.3-8\text{keV}} \gtrsim 4 \times 10^{-15} \text{ erg s}^{-1} \text{ cm}^{-2}$ are ruled out with 2σ confidence in all cases, with the possible exception of ESO 501-23 (see §3.7). The corresponding luminosities for each galaxy are shown in column 11 of Table 1. In addition, we stacked the galactic nuclei to search for a cumulative detection, but none was found.

4.2. The ULXs in NGC 337

There are 8 sources within the inner $1'$ of NGC 337 that have fluxes comparable to ULXs at a distance of 20.7 Mpc (see Figure 1). These include all NGC 337 sources listed in Table 7, except for X-2 and X-10. Based on M03, we expect ~ 0.35 background sources in the central arcminute above the ULX threshold. It is therefore very likely that all eight of these candidates are ULXs associated with NGC 337. In addition, 7 of the 8 objects coincide with H α emission, strengthening the ULX interpretation (Swartz et al. 2009). The 2σ detection limit of our *Chandra* image is $6 \times 10^{38} \text{ erg s}^{-1}$, lower than the ULX lower bound of $10^{39} \text{ erg s}^{-1}$. Therefore our

sample represents the full population of ultraluminous objects present in the galaxy at the time the data were taken. However, the large variability of ULX luminosities, in some cases over orders of magnitude (Middleton et al. 2012), implies that future observations could reveal new ultraluminous X-ray sources.

We can use our observations to evaluate the star formation properties of NGC 337. G03 describe a correlation between a galaxy's star formation rate (SFR) and the luminosity function (LF) of its high mass X-ray binaries, defined in this case as X-ray binaries with a massive stellar companion, and an X-ray luminosity $> 2 \times 10^{38} \text{ erg s}^{-1}$. This can be explained as a result of X-ray binaries created during epochs of star formation that accrete their companions on a timescale similar to the lifetime of star formation indicators. They found that the LF was best fit by a cut-off power law scaled linearly with SFR:

$$\frac{dN}{dL_{38}} = (3.3_{-0.8}^{+1.1}) \text{ SFR } L_{38}^{-1.61 \pm 0.12} \quad \text{for } L < L_C \quad (1)$$

$$N(> L) = 5.4 \text{ SFR } (L_{38}^{-0.61} - 210^{-0.61}) \quad (2)$$

Here, SFR is in units of $M_\odot \text{ yr}^{-1}$, $L_C \sim 2 \times 10^{40} \text{ erg s}^{-1}$, and $L_{38} \equiv \frac{L}{10^{38} \text{ erg s}^{-1}}$. The upper bound of L_C is a result of the observed power law break in the HMXB LF above $\sim 2 \times 10^{40} \text{ erg s}^{-1}$ (e.g. Swartz et al. 2011). The substantial error bars in Eq. (1) encompass several effects. One such effect is the inhomogeneity of HMXB LFs used to derive this relation. G03 took ULX luminosities directly from the literature for the galaxies considered in their study. Each study had its own methods of determining the target galaxy's HMXB LF (see the references in Table 1 of G03 for more information), though most assumed an absorbed power law. Band passes ranged from 0.7-7 keV to 0.1-10 keV, and several different spectral indices were used. This leads to a scatter in inferred flux for a fixed count rate. Another effect is the treatment of extinction. In most cases, Galactic hydrogen was the only extinguishing medium accounted for. This ignores absorption internal to the target galaxy, which may contribute to net extinction and spectral hardening. To complicate matters further, this can vary significantly between objects within the same galaxy. Uncertainties in galactic distances and star formation rates also contribute, and may be the dominate sources of error. Considering these effects, G03 found an error in derived star formation rate of $\sim 50\%$. Mineo, Gilfanov and Sunyaev (2012) recently repeated this analysis with closer attention to the systematic errors affecting G03, but found nearly the same uncertainty in derived SFR, implying this scatter may be real. With this precaution, we can proceed using the relation of G03.

To derive the HMXB LF, we choose a band-pass of 0.3-8 keV, a spectral index of 1.7, and Galactic absorption. This falls roughly in the middle of the literature range studied by G03. Only sources with $L_X > 6 \times 10^{38} \text{ erg s}^{-1}$ are considered to ensure completeness, though we note this may contribute to our total error. Using a maximum likelihood fit, we determine a SFR of $6.8_{-3.5}^{+4.4} M_\odot \text{ yr}^{-1}$. Figure 3 shows the HMXB luminosity function of NGC 337, along with realizations of Eq.(2) for three SFRs. To evaluate whether background contaminants could affect this value, we randomly subtracted single

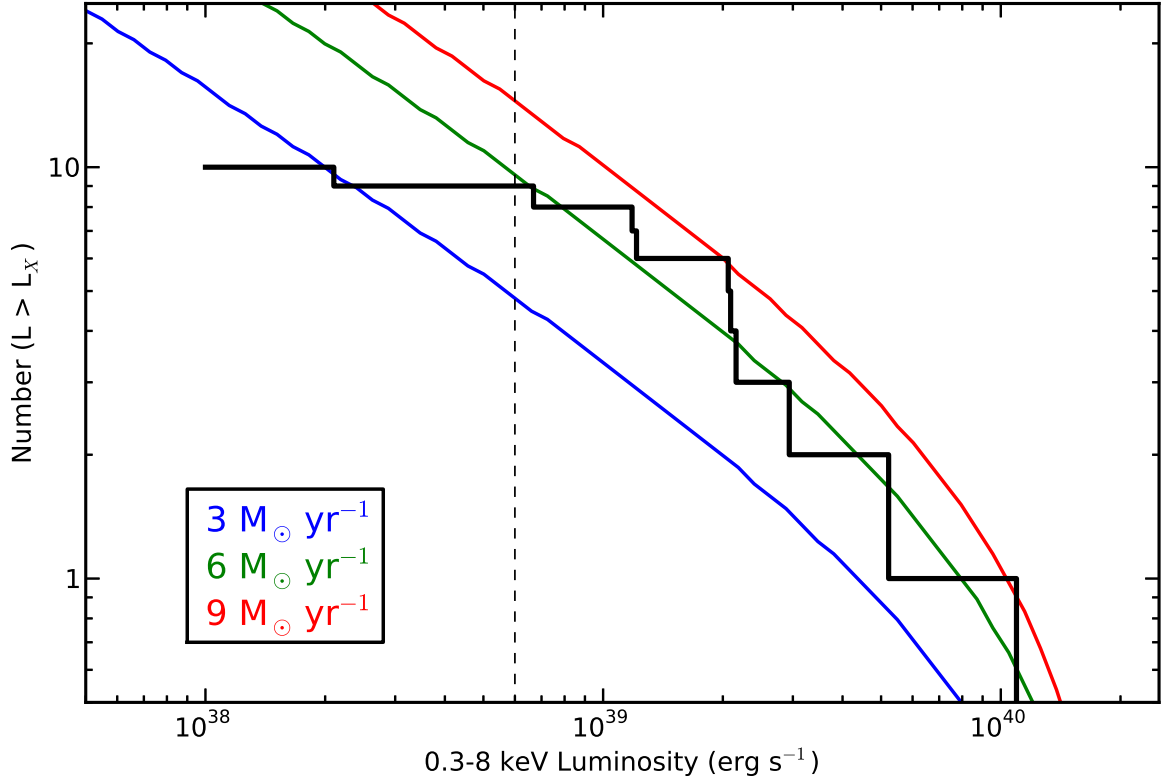


FIG. 3.— X-ray luminosity function of NGC 337, in black. X-ray luminosity values are determined with a power law with galactic absorption, $\Gamma = 1.7$, and a band-pass of 0.3–8 keV. Over-plotted are 3 realizations of Eq. (2), for star formation rates of 3, 6, and $9 \text{ M}_\odot \text{ yr}^{-1}$.

objects from the LF and re-derived the best fit. We found that the change in derived star formation rate was at most $1 \text{ M}_\odot \text{ yr}^{-1}$. This is a small effect compared to the systematic uncertainties, and likely even smaller since the most probable contaminants are lower flux sources which do not affect the LF as dramatically.

We can compare this estimate with SFRs derived from photometric indicators. G03 used the H α and far-IR SFR relations of Rosa-González et al. (2002), so we employ these for consistency. Watson et al. (2012) and Kennicutt & Moustakas (2006) found an extinction-corrected H α flux of $1.86 \times 10^{-12} \text{ erg s}^{-1} \text{ cm}^{-2}$, and $3.86 \times 10^{-12} \text{ erg s}^{-1} \text{ cm}^{-2}$, giving $\text{SFR(H}\alpha\text{)} \sim 1.0$ and $2.2 \text{ M}_\odot \text{ yr}^{-1}$, respectively. The far-IR luminosity measurement of Sanders et al. (2003), rescaled to a distance of 20.7 Mpc, gives a luminosity of $\sim 4.1 \times 10^{43} \text{ erg s}^{-1}$. This implies $\text{SFR(FIR)} \sim 1.9 \text{ M}_\odot \text{ yr}^{-1}$. Extinction in the FIR is minimal, so we do not correct our estimate. To determine if these values are consistent with a state-of-the-art calculation, we rescaled the recent analysis of *Spitzer* and H α images by Calzetti et al. (2012) to our adopted distance. This gives $\text{SFR} = 1.50_{-0.31}^{+0.39} \text{ M}_\odot \text{ yr}^{-1}$, consistent with the range implied by the calibrations of Rosa-González et al. (2002), and consistent with our HMXB-determined SFR at $\sim 1.5\sigma$. Although not a highly significant difference, one explanation for this offset may be the incompleteness of this sample of HMXBs. G03 was derived for all binaries above $2 \times 10^{38} \text{ erg s}^{-1}$, whereas our completeness limit is $6 \times 10^{38} \text{ erg s}^{-1}$. A deeper observation of NGC 337 will complete the luminosity function down

to lower limit used by G03, and allow for a more precise application of this correlation. Another possibility proposed by Shields et al. (2012) is that a significant discrepancy between SFR indicators and G03 may be seen if a galaxy is near the conclusion of a star burst epoch. In this scenario, HMXBs and ULXs have outlived classic SFR indicators, which have been attenuated as the stellar population ages. However, with a weak significance of only 1.5σ , the high abundance of HMXBs in NGC 337 is likely a statistical fluctuation rather than a galaxy observed in a special epoch. Nevertheless, NGC 337 hosts a rich population of ULX candidates and may prove valuable to the ongoing study of ultraluminous X-ray sources.

4.3. ESO 501-23 X-1

ESO 501-23 X-1 is located at R.A. = $10^{\text{h}}35^{\text{m}}22.2^{\text{s}}$, Dec. = $-24^{\circ}45^{\prime}14^{\prime\prime}$. It is the brightest source discovered in this study, with a net count rate of $\approx 0.087 \pm 0.003 \text{ cts s}^{-1}$ within a $2.3''$ aperture. By inspection, we find a significant excess of photons above the background surrounding this extraction circle. We therefore include counts within $4.6''$ of the source centroid, double the original extraction circle, and find a marginally higher rate of $0.090 \pm 0.003 \text{ cts s}^{-1}$. The resulting spectrum is shown in Figure 5. We fit this spectrum with a power law including Galactic absorption (Kalberla et al. 2005), and a second variable absorption term. This produced a good fit to the spectrum ($\Gamma = 1.18_{-0.11}^{+0.19}$, $N_{\text{H}} = 1.13_{-1.13}^{+7.07} \times 10^{20} \text{ cm}^{-2}$, norm = $8.89_{-0.94}^{+1.90} \times 10^{-5}$, $\chi_{\text{red}}^2 = 1.089$ for 38

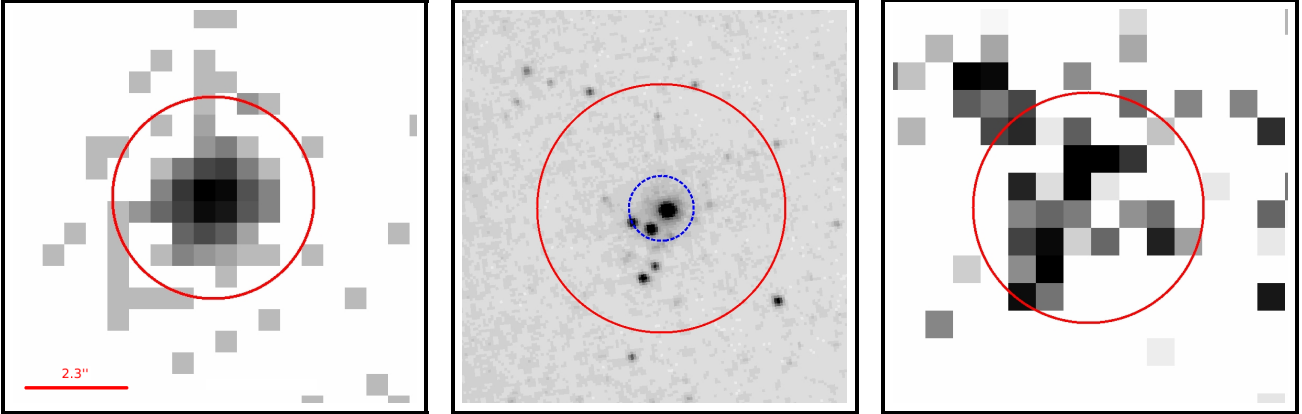


FIG. 4.— *Left:* Unsmoothed image of ESO 501-23 X-1 from *Chandra*. The red circle has a radius of $2.3''$, equal to half the extraction circle. *Middle:* HST WFC1 F606W image of X-1. The red circle has a radius of $2.3''$, and the blue circle has a radius of $0.6''$, equal to the *Chandra* 90% source certainty region. *Right:* $\text{H}\alpha$ image of X-1 from MDM 2.4m imaging.

d.o.f.), and gives an unabsorbed flux of $1.08^{+0.05}_{-0.07} \times 10^{-12}$ $\text{erg s}^{-1} \text{cm}^{-2}$. Errors quoted are 90% confidence intervals. Other simple models do not perform as well, but produce fluxes within $\sim 7\%$ of this value. CXB sources with a flux this large are rare, with M03 estimating 0.02 seen within the collective D25s of our sample. Although distance estimates vary considerably, they all imply an X-ray luminosity $> 5 \times 10^{39} \text{ erg s}^{-1}$ for X-1. Considering its spectral shape, brightness, off-axis position, and coincidence with $\text{H}\alpha$ emission (Figure 4), this is likely a *bona fide* ULX.

Power laws have been widely used to model ultraluminous X-ray sources in the literature and typically describe their spectra well, but lack the complexity to accurately reflect ULX spectra with sampling in excess of $\sim 10,000$ counts (Gladstone et al. 2009). This demonstrates the need for high quality data if one plans to make accurate inferences about the source’s physical nature. With only ~ 800 counts, we cannot discriminate between more complicated spectral models, and thus do not attempt an analysis of this object in the context of the ULX progenitor debate. A deeper exposure with a higher effective area spectrograph, such as the *EPIC* instrument aboard *XMM-Newton*, could shed light on this promising object.

Although we do not speculate on the mass of X-1’s putative black hole, we can use its spectral index to constrain its luminosity. Berghea et al. (2008) assembled a sample of ULXs to study their collective properties, showing in particular a negative correlation between spectral hardness and X-ray luminosity. The evidence for this relation was strengthened by Sutton et al. (2012), who reprocessed the Berghea sample luminosities using best-fit power law spectral parameters. They found $\langle \Gamma \rangle = 2.10 \pm 0.07$ for ULXs with $L_X < 10^{40} \text{ erg s}^{-1}$, and $\langle \Gamma \rangle = 1.54 \pm 0.06$ for ULXs with $L_X > 10^{40} \text{ erg s}^{-1}$. If ESO 501-23 X-1 follows this pattern, its spectral index of $\Gamma \approx 1.2^{+0.2}_{-0.1}$ implies $L_X > 10^{40} \text{ erg s}^{-1}$. We can use this prior to evaluate distance estimates to ESO 501-23, which show scatter at the factor of 2 level. Tully (1988) and (2008) give 14.2 Mpc and 7.01 Mpc respectively, and Virgo infall-corrected redshift measurements give ~ 13 Mpc (Mould et al. 2000), assuming standard cosmology ($H_0 = 70 \text{ km s}^{-1} \text{ Mpc}^{-1}$). The closest of these estimates gives an unabsorbed luminosity of $L_X = 6.4^{+0.3}_{-0.4} \times 10^{39} \text{ erg s}^{-1}$ for X-1, securely in the ULX regime. However,

if this is the correct distance to the galaxy, X-1 would be one of the hardest $L_X < 10^{40} \text{ erg s}^{-1}$ ULXs yet discovered. We do not rule out this possibility, as there is a large intrinsic scatter in Γ for dimmer ULXs (see Figure 6 in Sutton et al. 2012). However, the more distant estimates imply a luminosity of $\gtrsim 2 \times 10^{40} \text{ erg s}^{-1}$ for X-1, a value much more consistent with the findings of Sutton et al. (2012). Although we cannot resolve this disagreement, our observations favor the larger distance calculations.

We searched archival HST data for a potential counterpart to this source. Only a F606W ACS/WFC image of the source position exists in the archive, shown in Figure 4. This image reveals multiple bright optical sources within the *Chandra* positional error circle, with a diffuse light occupying a radius of ~ 100 parsecs. This may imply that X-1 is a collection of bright X-ray point sources that together reach an ultraluminous level. Further X-ray observations of X-1 could disfavor this interpretation if substantial variability is detected. Alternatively, the brightest source in the HST image could be a high mass stellar companion of an accreting black hole or a tight stellar population in which the ULX resides, both of which have been claimed for other ULXs (e.g. Roberts et al. 2008, Farrell et al. 2012). Additionally, the diffuse light surrounding this object may be explained by a circum-ULX nebula, which has been reported in some cases (e.g. Pakull & Mirioni 2003), or could simply be blended light from low mass stars. Future spectroscopic and color information could help discriminate between these possibilities, and add to statistics about ULX companions and environments.

5. CONCLUSIONS

Drawing from the sample of W11, we select eight bulgeless disk galaxies for study using the *Chandra* X-ray Observatory. We report the discovery of several strong ULX candidates in the star forming galaxy NGC 337, which imply an SFR of $6.8^{+4.4}_{-3.5} \text{ M}_\odot \text{ yr}^{-1}$. This is consistent at $\sim 1.5\sigma$ with the current best estimate of the star formation rate of NGC 337, and may be made more consistent with a higher signal-to-noise determination of its HMXB luminosity function. We discovered a bright X-ray source in the galaxy ESO 501-23, and argue that it is a *bona fide* ULX based on its flux, spectrum, off-center location, and coincidence with $\text{H}\alpha$. Its spectral index im-

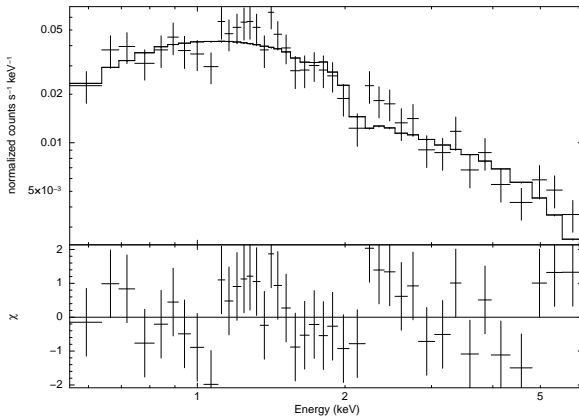


FIG. 5.— ESO 501-23 X-1 spectrum extracted from a 4.6'' radius circle and binned to include at least 20 counts per tick. Also plotted is the best fit absorbed power law model described in §4.2, and the χ^2 residuals of each bin.

plies a luminosity $\gtrsim 10^{40}$ erg s $^{-1}$ which, if correct, argues the distance to ESO 501-23 is larger than some previous published estimates. Further investigation of this source may reveal the nature of its optical counterpart, which is seen in HST imaging. Additional ULX candidates are identified in IC 1291, PGC 3853, NGC 5964, and NGC 2805, though deeper X-ray observations are required to adequately model their spectra. None of these galaxies appear active, confirming their optical classification in the literature, and supporting the notion that AGN in bulge-less spirals are rare. We also note that an X-ray source lies near the center of ESO 501-23, but do no claim that it is an AGN due to large uncertainties in the exact central coordinates of the galaxy. This source may warrant further attention in future X-ray studies of this galaxy. Finally, we do not detect the type II-P supernova SN 2011DQ, which exploded in NGC 337 prior to our observation.

REFERENCES

- Abramowicz, M. A., Czerny, B., Lasota, J. P., & Szuszkiewicz, E. 1988, ApJ, 332, 646
- Adelman-McCarthy, J. K., & et al. 2011, VizieR Online Data Catalog, 2306, 0
- Araya Salvo, C., Mathur, S., Ghosh, H., Fiore, F., & Ferrarese, L. 2012, ApJ, 757, 179
- Arnaud, K. A. 1996, Astronomical Data Analysis Software and Systems V, 101, 17
- Barbon, R., Buondi, V., Cappellaro, E., & Turatto, M. 2009, VizieR Online Data Catalog, 1, 2024
- Begelman, M. C. 2002, ApJ, 568, L97
- Belczynski, K., Bulik, T., Fryer, C. L., et al. 2010, ApJ, 714, 1217
- Berghea, C. T., Weaver, K. A., Colbert, E. J. M., & Roberts, T. P. 2008, ApJ, 687, 471
- Calzetti, D., Wu, S.-Y., Hong, S., et al. 2010, ApJ, 714, 1256
- Calzetti, D. 2012, arXiv:1208.2997
- Colbert, E. J. M., & Mushotzky, R. F. 1999, ApJ, 519, 89
- Copenhagen University, O., Institute, A. O., Cambridge, U.K., & Real Instituto Y Observatorio de La Armada, F. E. S. 2006, VizieR Online Data Catalog, 1304, 0
- Cutri, R. M., & et al. 2012, VizieR Online Data Catalog, 2311, 0
- Dalcanton, J. J., Yoachim, P., & Bernstein, R. A. 2004, ApJ, 608, 189
- Farrell, S. A., Webb, N. A., Barret, D., Godet, O., & Rodrigues, J. M. 2009, Nature, 460, 73
- Farrell, S. A., Servillat, M., Pforr, J., et al. 2012, ApJ, 747, L13
- Feng, H., & Soria, R. 2011, New Astron. Rev., 55, 166
- Ferrarese, L., & Merritt, D. 2000, ApJ, 539, L9
- Filippenko, A. V., & Ho, L. C. 2003, ApJ, 588, L13
- Fruscione, A., McDowell, J. C., Allen, G. E., et al. 2006, Proc. SPIE, 6270
- Gebhardt, K., Bender, R., Bower, G., et al. 2000, ApJ, 539, L13
- Ghosh, H., Mathur, S., Fiore, F., & Ferrarese, L. 2008, ApJ, 687, 216
- Ghosh, H. 2009, Ph.D. Thesis,
- Gladstone, J. C., Roberts, T. P., & Done, C. 2009, MNRAS, 397, 1836
- Grimm, H.-J., Gilfanov, M., & Sunyaev, R. 2003, MNRAS, 339, 793 (G03)
- Häring, N., & Rix, H.-W. 2004, ApJ, 604, L89
- Jones, D. H., Saunders, W., Colless, M., et al. 2004, MNRAS, 355, 747
- Jonker, P. G., Heida, M., Torres, M. A. P., et al. 2012, ApJ, 758, 28
- Kaaret, P. 2005, ApJ, 629, 233
- Kennicutt, R. C., Jr. 1998, ARA&A, 36, 189
- Kennicutt, R. C., Jr., Armus, L., Bendo, G., et al. 2003, PASP, 115, 928
- King, A. R., Davies, M. B., Ward, M. J., Fabbiano, G., & Elvis, M. 2001, ApJ, 552, L109
- King, A. R. 2004, MNRAS, 347, L18
- Kormendy, J., & Bender, R. 2011, Nature, 469, 377

Support for this work was provided by the National Aeronautics and Space Administration through Chandra Award Number GO1-12113X issued by the Chandra X-ray Observatory Center, which is operated by the Smithsonian Astrophysical Observatory for and on behalf of the National Aeronautics Space Administration under contract NAS8-03060. Funding for SDSS-III has been provided by the Alfred P. Sloan Foundation, the Participating Institutions, the National Science Foundation, and the U.S. Department of Energy Office of Science. The SDSS-III web site is <http://www.sdss3.org/>. SDSS-III is managed by the Astrophysical Research Consortium for the Participating Institutions of the SDSS-III Collaboration including the University of Arizona, the Brazilian Participation Group, Brookhaven National Laboratory, University of Cambridge, University of Florida, the French Participation Group, the German Participation Group, the Instituto de Astrofisica de Canarias, the Michigan State/Notre Dame/JINA Participation Group, Johns Hopkins University, Lawrence Berkeley National Laboratory, Max Planck Institute for Astrophysics, New Mexico State University, New York University, Ohio State University, Pennsylvania State University, University of Portsmouth, Princeton University, the Spanish Participation Group, University of Tokyo, University of Utah, Vanderbilt University, University of Virginia, University of Washington, and Yale University. This publication makes use of data products from the Wide-field Infrared Survey Explorer, which is a joint project of the University of California, Los Angeles, and the Jet Propulsion Laboratory/California Institute of Technology, funded by the National Aeronautics and Space Administration. This research has made use of the USNO Image and Catalogue Archive operated by the United States Naval Observatory, Flagstaff Station (<http://www.nofs.navy.mil/data/fchpix/>). GS would like to thank Dale Mudd for his helpful comments.

- Liu, J.-F., Bregman, J. N., & Seitzer, P. 2004, ApJ, 602, 249
- Mathur, S., Fields, D., Peterson, B. M., & Grupe, D. 2012, ApJ, 754, 146
- Menci, N., Fiore, F., Perola, G. C., & Cavaliere, A. 2004, ApJ, 606, 58
- Miller, M. C., & Colbert, E. J. M. 2004, International Journal of Modern Physics D, 13, 1
- Mineo, S., Gilfanov, M., & Sunyaev, R. 2012, arXiv:1207.2157
- Monet, D. G., Levine, S. E., Canzian, B., et al. 2003, AJ, 125, 984
- Moretti, A., Campana, S., Lazzati, D., & Tagliaferri, G. 2003, ApJ, 588, 696 (M03)
- Mould, J. R., Huchra, J. P., Freedman, W. L., et al. 2000, ApJ, 529, 786
- Moustakas, J., & Kennicutt, R. C., Jr. 2006, ApJS, 164, 81
- Pakull, M. W., & Mirioni, L. 2002, arXiv:astro-ph/0202488
- Pakull, M. W., & Mirioni, L. 2003, Revista Mexicana de Astronomia y Astrofisica Conference Series, 15, 197
- Paturel, G., Petit, C., Prugniel, P., et al. 2003, A&A, 412, 45
- Pooley, D., & Lewin, W. H. G. 2004, IAU Circ., 8390, 1
- Poutanen, J., Lipunova, G., Fabrika, S., Butkevich, A. G., & Abolmasov, P. 2007, MNRAS, 377, 1187
- Remillard, R. A., & McClintock, J. E. 2006, ARA&A, 44, 49
- Roberts, T. P. 2007, Ap&SS, 311, 203
- Roberts, T. P., Levan, A. J., & Goad, M. R. 2008, MNRAS, 387, 73
- Rosa-González, D., Terlevich, E., & Terlevich, R. 2002, MNRAS, 332, 283
- Sandage, A., & Bedke, J. 1994, The Carnegie Atlas of Galaxies. Volumes I, II., by Sandage, A.; Bedke, J.. Carnegie Institution of Washington Publ., No. 638,,
- Sanders, D. B., Mazzarella, J. M., Kim, D.-C., Surace, J. A., & Soifer, B. T. 2003, AJ, 126, 1607
- Satyapal, S., Vega, D., Heckman, T., O'Halloran, B., & Dudik, R. 2007, ApJ, 663, L9
- Secrest, N. J., Satyapal, S., Gliozzi, M., et al. 2012, ApJ, 753, 38
- Shakura, N. I., & Sunyaev, R. A. 1973, A&A, 24, 337
- Shields, J. C., Walcher, C. J., Böker, T., et al. 2008, IAU Symposium, 245, 259
- Shields, J. C., Böker, T., Ho, L. C., et al. 2012, AJ, 144, 12
- Swartz, D. A., Tennant, A. F., & Soria, R. 2009, ApJ, 703, 159
- Swartz, D. A., Soria, R., Tennant, A. F., & Yukita, M. 2011, ApJ, 741, 49
- Tully, R. B., & Fisher, J. R. 1988, Catalog of Nearby Galaxies, by R. Brent Tully and J. Richard Fisher, pp. 224. ISBN 0521352991. Cambridge, UK: Cambridge University Press, April 1988.,
- Tully, R. B., Rizzi, L., Shaya, E. J., et al. 2009, AJ, 138, 323
- Watarai, K.-y., Fukue, J., Takeuchi, M., & Mineshige, S. 2000, PASJ, 52, 133
- Watson, L. C., Schinnerer, E., Martini, P., Böker, T., & Lisenfeld, U. 2011, ApJS, 194, 36
- Watson, L. C., Martini, P., Lisenfeld, U., et al. 2012, ApJ, 751, 123
- Weisskopf, M. C., Tananbaum, H. D., Van Speybroeck, L. P., & O'Dell, S. L. 2000, Proc. SPIE, 4012, 2
- Winter, L. M., Mushotzky, R. F., & Reynolds, C. S. 2006, ApJ, 649, 730
- Wright, E. L., Eisenhardt, P. R. M., Mainzer, A. K., et al. 2010, AJ, 140, 1868
- Yuan, H.-B., Liu, X.-W., & Xiang, M.-S. 2013, arXiv:1301.1427

TABLE 1
GALAXY PROPERTIES

Galaxy Name (1)	R.A. (J2000) (2)	Dec. (J2000) (3)	Error ('') (4)	Dist. (Mpc) (5)	Ma. ('') (6)	Mi. ('') (7)	P.A. (°) (8)	Type (T) (9)	N_H ($\times 10^{20}$) (10)	AGN Limit (11)
NGC 337	00:59:50.09	-07:34:40.7	1.25	20.7 [T88]	173	109	118 ± 5	7.0	7.34	38.27
IC 1291	18:33:52.57	+49:16:43.0	1.25	31.5 [T88]	109	91	131 ± 2	8.0	5.55	38.62
PGC 3853	01:05:04.88	-06:12:44.6	1.25	11.4 [T08]	250	213	105.3 ± 0.2	7.0	5.11	37.92
NGC 5964	15:37:36.32	+05:58:24.3	1.25	24.7 [T88]	250	194	136.7 ± 1.2	7.0	4.29	38.40
UGC 6446	11:26:40.46	+53:44:48.3	0.50	18.0 [T08]	213	137	189.4 ± 0.5	7.0	0.97	38.09
NGC 2805	09:20:20.41	+64:06:10.0	1.25	28.0 [T88]	379	287	300 ± 3	7.0	4.01	38.52
ESO 501-23	10:35:23.20	-24:45:14.9	1.25	7.01 [T08]	208	165	224 ± 2	8.0	4.58	37.31
NGC 3794	11:40:54.24	+56:12:07.2	0.50	19.2 [T08]	134	87	123.1 ± 1.1	6.5	0.92	38.15

NOTE. — Column 1: Galaxy name. Columns 2, 3 and 4: R.A. and Dec. of galactic nucleus with uncertainties, taken from 2MASS, SDSS (UGC6446, NGC3794) and 6dF (ESO501-23). These are typically photometric centers; see W11 for rotational centers. Column 5: Distance to the galaxy from Tully et al. (1988, [T88]) or (2008, T[08]) as indicated. Columns 6 and 7: Semi-major and semi-minor axes of the 25th magnitude arcsec⁻² B-band isophote from de Vaucouleurs et al. (1991). Column 8: Pitch angle of the galaxy, from Watson et al. (2012). Column 9: De Vaucouleurs T Type. Column 10: Galactic hydrogen column density per cm² along line-of-sight to galaxy from Kalberla et al. (2005). Column 11: Log 2 σ upper limit for a putative AGN luminosity at the location from Columns 2 and 3.

TABLE 2
OBSERVATIONS

Galaxy (1)	R.A. (J2000) (2)	Dec. (J2000) (3)	Obs ID (4)	Observation Date (yyyy-mm-dd) (5)	Exposure (ks) (6)	Chip (7)	Filtered Time (ks) (8)
NGC 337	00:59:50.1	-07:34:41	12979	2011-07-19	9.93	S2 S3 S4	9.61 9.93 N/A
IC 1291	18:33:52.6	+49:16:43	12980	2011-04-06	9.93	S2 S3 S4	8.98 9.93 8.66
PGC 3853	01:05:04.9	-06:12:45	12981	2011-06-26	9.93	S2 S3 S4	9.47 9.81 9.79
NGC 5964	15:37:36.3	+05:58:24	12982	2011-04-19	9.93	S2 S3 S4	9.23 9.93 9.23
UGC 6446	11:26:40.4	+53:44:51	12983	2012-01-17	9.93	S2 S3 S4	8.98 9.93 N/A
NGC 2805	09:20:20.4	+64:06:10	12984	2011-11-06	9.93	S2 S3 S4	8.91 9.61 8.66
ESO 501-23	10:35:23.2	-24:45:09	12985	2010-11-09	9.93	S2 S3 S4	8.82 9.93 9.61
NGC 3794	11:40:53.4	+56:12:07	12986	2012-01-18	9.93	S2 S3 S4	9.85 9.93 8.84

NOTE. — Column 1: Galaxy name. Columns 2 and 3: J2000 R.A. and Dec. of the pointing location of the observation. Column 4: *Chandra* observation ID. Column 5: Date of observation. Column 6: Unfiltered observation time in kiloseconds. Columns 7 and 8: The respective time filter for each ACIS-S chip. N/A implies that no sources were detected on the chip, and thus no time filter was applied.

TABLE 3
FULL SOURCE LIST

Obs ID	Chip Num	ID Num	Source Name (CXOU)	R.A. (J2000)	Decl. (J2000)	A_{eff} (cm 2)	Δ ($'$)	Net Counts \pm Error (0.3-8 keV)	Soft Counts \pm Error (0.3-2 keV)	Hard Counts \pm Error (2-8 keV)	Inside D25?
(1)	(2)	(3)	(4)	(5)	(6)	(7)	(8)	(9)	(10)	(11)	(12)
12979	S2	1	J005951.7-073052	00 59 51.7	-07 30 52	589	3.7	14.7 \pm 3.9	14.0 \pm 3.7	0.7 \pm 1.0	...
		2	J005951.5-073134	00 59 51.5	-07 31 34	597	3.0	10.8 \pm 3.3	4.0 \pm 2.0	6.9 \pm 2.6	...
		3	J005944.6-073058	00 59 44.6	-07 30 58	587	3.7	8.8 \pm 3.0	3.9 \pm 2.0	4.9 \pm 2.2	...
		4	J005937.3-073034	00 59 37.3	-07 30 34	486	4.9	9.2 \pm 3.2	3.7 \pm 2.0	5.6 \pm 2.5	...
		5	J005952.3-073447	00 59 52.3	-07 34 47	628	0.8	43.8 \pm 6.7	32.3 \pm 5.7	11.5 \pm 3.5	Y
	S3	6	J005951.9-073458	00 59 51.9	-07 34 58	589	0.8	14.0 \pm 3.9	4.5 \pm 2.2	9.5 \pm 3.2	Y
		7	J005950.6-073458	00 59 50.6	-07 34 58	627	0.6	315.4 \pm 17.8	194.8 \pm 14.0	120.6 \pm 11.0	Y
		8	J005950.4-073454	00 59 50.4	-07 34 54	627	0.5	43.2 \pm 6.7	26.7 \pm 5.3	16.5 \pm 4.1	Y
		9	J005949.5-073523	00 59 49.5	-07 35 23	653	0.9	24.8 \pm 5.0	18.0 \pm 4.2	6.9 \pm 2.6	Y
		10	J005949.5-073436	00 59 49.5	-07 34 36	654	0.1	109.3 \pm 10.5	64.7 \pm 8.1	44.7 \pm 6.7	Y
		11	J005948.5-073457	00 59 48.5	-07 34 57	623	0.5	61.5 \pm 7.9	41.7 \pm 6.5	19.8 \pm 4.5	Y
		12	J005947.5-073417	00 59 47.5	-07 34 17	649	0.5	45.2 \pm 6.8	41.7 \pm 6.5	3.5 \pm 2.0	Y
		13	J005940.5-073348	00 59 40.5	-07 33 48	636	2.3	60.8 \pm 7.8	43.9 \pm 6.6	16.9 \pm 4.1	...
		14	J005953.3-073521	00 59 53.3	-07 35 21	653	1.3	25.4 \pm 5.1	14.5 \pm 3.9	11.0 \pm 3.3	Y
		15	J005953.3-073457	00 59 53.3	-07 34 57	654	1.1	4.4 \pm 2.2	2.7 \pm 1.7	1.7 \pm 1.4	Y
		16	J005948.1-073808	00 59 48.1	-07 38 08	634	3.7	27.8 \pm 5.3	22.8 \pm 4.8	5.0 \pm 2.2	...
		17	J005954.6-073656	00 59 54.6	-07 36 56	609	2.8	6.7 \pm 2.6	5.9 \pm 2.5	0.9 \pm 1.0	...
		18	J005943.5-073501	00 59 43.5	-07 35 01	647	1.5	8.9 \pm 3.0	7.0 \pm 2.6	1.9 \pm 1.4	...
		19	J010007.3-073522	01 00 07.3	-07 35 22	386	4.6	18.1 \pm 4.5	9.0 \pm 3.2	9.1 \pm 3.2	...
		20	J005956.4-073832	00 59 56.4	-07 38 32	631	4.4	9.0 \pm 3.2	4.6 \pm 2.2	4.3 \pm 2.2	...
		21	J005935.4-073621	00 59 35.4	-07 36 21	606	3.9	4.7 \pm 2.2	2.8 \pm 1.7	1.9 \pm 1.4	...
12980	S2	22	J183353.7+491904	18 33 53.7	+49 19 04	502	2.2	7.8 \pm 2.8	6.0 \pm 2.4	1.8 \pm 1.4	...
		23	J183347.6+491946	18 33 47.6	+49 19 46	588	3.2	6.7 \pm 2.6	4.9 \pm 2.2	1.9 \pm 1.4	...
		24	J183400.8+492028	18 34 00.8	+49 20 28	588	3.9	8.9 \pm 3.0	9.0 \pm 3.0	-0.1 \pm 0.1	...
		25	J183344.1+492109	18 33 44.1	+49 21 09	579	4.4	13.5 \pm 3.7	7.9 \pm 2.8	5.7 \pm 2.5	...
		26	J183327.7+491816	18 33 27.7	+49 18 16	530	4.1	9.7 \pm 3.2	4.8 \pm 2.2	4.9 \pm 2.2	...
		27	J183412.1+492155	18 34 12.1	+49 21 55	436	6.0	17.4 \pm 4.4	10.3 \pm 3.3	7.0 \pm 2.8	...
		28	J183346.6+492136	18 33 46.6	+49 21 36	576	4.7	9.6 \pm 3.2	4.8 \pm 2.2	4.8 \pm 2.2	...
		29	J183340.9+492251	18 33 40.9	+49 22 51	558	6.2	12.2 \pm 3.8	6.5 \pm 2.7	5.7 \pm 2.7	...
		30	J183356.5+492343	18 33 56.5	+49 23 43	495	6.8	16.5 \pm 4.3	8.6 \pm 3.0	7.9 \pm 3.0	...
	S3	31	J183402.2+491817	18 34 02.2	+49 18 17	640	2.2	346.1 \pm 18.6	221.7 \pm 14.9	124.4 \pm 11.2	...
		32	J183355.8+491746	18 33 55.8	+49 17 46	649	1.1	72.8 \pm 8.5	33.9 \pm 5.8	38.9 \pm 6.2	...
		33	J183351.5+491642	18 33 51.5	+49 16 42	654	0.2	28.5 \pm 5.4	25.7 \pm 5.1	2.8 \pm 1.7	Y
		34	J183347.0+491423	18 33 47.0	+49 14 23	641	2.6	80.7 \pm 9.0	58.8 \pm 7.7	21.9 \pm 4.7	...
		35	J183333.4+491617	18 33 33.4	+49 16 17	627	3.0	64.6 \pm 8.1	46.8 \pm 6.9	17.9 \pm 4.2	...
		36	J183416.4+491544	18 34 16.4	+49 15 44	622	4.2	62.9 \pm 8.0	26.5 \pm 5.2	36.3 \pm 6.1	...
		37	J183350.6+491558	18 33 50.6	+49 15 58	652	1.0	10.6 \pm 3.3	8.8 \pm 3.0	1.8 \pm 1.4	Y
		38	J183355.5+491741	18 33 55.5	+49 17 41	648	1.0	8.7 \pm 3.0	5.8 \pm 2.5	2.9 \pm 1.7	...
		39	J183346.1+491711	18 33 46.1	+49 17 11	646	0.9	4.6 \pm 2.2	3.9 \pm 2.0	0.7 \pm 1.0	...
		40	J183415.8+491242	18 34 15.8	+49 12 42	534	5.8	28.8 \pm 5.5	23.4 \pm 4.9	5.3 \pm 2.5	...
		41	J183355.3+491527	18 33 55.3	+49 15 27	652	1.6	6.2 \pm 2.7	3.8 \pm 2.0	2.4 \pm 1.7	...
		42	J183351.4+491332	18 33 51.4	+49 13 32	637	3.4	8.8 \pm 3.0	4.0 \pm 2.0	4.8 \pm 2.2	...
		43	J183327.0+491736	18 33 27.0	+49 17 36	599	4.0	9.6 \pm 3.2	8.9 \pm 3.0	0.7 \pm 1.0	...
		44	J183331.7+491417	18 33 31.7	+49 14 17	608	4.2	9.8 \pm 3.3	9.6 \pm 3.2	0.2 \pm 1.0	...
		45	J183330.8+491216	18 33 30.8	+49 12 16	288	5.8	11.8 \pm 3.6	6.3 \pm 2.7	5.5 \pm 2.5	...
		46	J183336.4+490950	18 33 36.4	+49 09 50	578	7.5	13.9 \pm 4.0	8.2 \pm 3.0	5.7 \pm 2.7	...
S4	47	J183410.5+490933	18 34 10.5	+49 09 33	476	8.0	10.5 \pm 3.5	6.6 \pm 2.6	3.9 \pm 2.2	...	

TABLE 3
CONTINUED

Obs ID	Chip Num	ID Num	Source Name (CXOU)	R.A. (J2000)	Decl. (J2000)	A_{eff} (cm 2)	Δ ($'$)	Net Counts \pm Error (0.3-8 keV)	Soft Counts \pm Error (0.3-2 keV)	Hard Counts \pm Error (2-8 keV)	Inside D25?
(1)	(2)	(3)	(4)	(5)	(6)	(7)	(8)	(9)	(10)	(11)	(12)
12981	S2	48	J010509.0-060650	01 05 09.0	-06 06 50	559	5.9	21.4 \pm 4.7	16.9 \pm 4.1	4.5 \pm 2.2	...
		49	J010454.3-060622	01 04 54.3	-06 06 22	553	6.7	6.1 \pm 2.8	3.4 \pm 2.0	2.7 \pm 2.0	...
		50	J010443.6-060808	01 04 43.6	-06 08 08	546	6.7	31.4 \pm 5.8	22.5 \pm 4.8	8.9 \pm 3.2	...
		51	J010442.2-060712	01 04 42.2	-06 07 12	536	7.6	28.7 \pm 5.5	19.5 \pm 4.5	9.2 \pm 3.2	...
		52	J010511.3-061207	01 05 11.3	-06 12 07	652	1.9	182.6 \pm 13.5	130.8 \pm 11.4	51.8 \pm 7.2	Y
	S3	53	J010506.5-061509	01 05 06.5	-06 15 09	567	2.6	21.0 \pm 4.6	16.0 \pm 4.0	5.0 \pm 2.2	...
		54	J010502.8-061536	01 05 02.8	-06 15 36	598	3.0	18.5 \pm 4.4	14.7 \pm 3.9	3.9 \pm 2.0	...
		55	J010502.6-061509	01 05 02.6	-06 15 09	642	2.6	12.7 \pm 3.6	8.9 \pm 3.0	3.9 \pm 2.0	...
		56	J010514.0-061028	01 05 14.0	-06 10 28	582	3.3	9.8 \pm 3.2	8.0 \pm 2.8	1.8 \pm 1.4	...
		57	J010504.5-061323	01 05 04.5	-06 13 23	653	0.8	4.6 \pm 2.2	4.8 \pm 2.2	-0.2 \pm 0.1	Y
		58	J010516.1-061749	01 05 16.1	-06 17 49	612	6.0	45.3 \pm 7.0	32.3 \pm 5.8	13.0 \pm 3.9	...
		59	J010500.2-061540	01 05 00.2	-06 15 40	634	3.2	4.8 \pm 2.2	2.0 \pm 1.4	2.8 \pm 1.7	...
		60	J010522.4-061252	01 05 22.4	-06 12 52	614	4.6	14.5 \pm 4.0	9.2 \pm 3.2	5.2 \pm 2.5	...
		61	J010522.2-061152	01 05 22.2	-06 11 52	102	4.6	5.2 \pm 2.5	4.8 \pm 2.2	0.4 \pm 1.0	...
		62	J010515.5-061639	01 05 15.5	-06 16 39	583	5.0	6.5 \pm 2.8	5.2 \pm 2.5	1.3 \pm 1.4	...
12982	S4	63	J010523.5-061250	01 05 23.5	-06 12 50	322	4.9	8.3 \pm 3.2	5.0 \pm 2.5	3.3 \pm 2.0	...
		64	J010517.0-061825	01 05 17.0	-06 18 25	599	6.7	13.4 \pm 4.1	8.4 \pm 3.2	5.1 \pm 2.7	...
		65	J010513.9-061750	01 05 13.9	-06 17 50	614	5.8	8.3 \pm 3.0	7.0 \pm 2.6	1.4 \pm 1.4	...
		66	J010505.3-061148	01 05 05.3	-06 11 48	648	0.9	4.8 \pm 2.2	3.0 \pm 1.7	1.8 \pm 1.4	Y
		67	J010529.6-061734	01 05 29.6	-06 17 34	214	8.1	10.8 \pm 3.6	5.9 \pm 2.7	4.9 \pm 2.5	...
		68	J010523.5-062029	01 05 23.5	-06 20 29	512	9.3	12.8 \pm 4.3	3.7 \pm 2.2	9.0 \pm 3.6	...
		69	J010513.1-062151	01 05 13.1	-06 21 51	530	9.5	19.0 \pm 5.0	6.6 \pm 2.8	12.5 \pm 4.1	...
		70	J153734.2+060131	15 37 34.2	+06 01 31	597	3.0	11.9 \pm 3.5	7.0 \pm 2.6	4.9 \pm 2.2	...
		71	J153727.6+060025	15 37 27.6	+06 00 25	596	2.7	10.0 \pm 3.2	9.0 \pm 3.0	1.0 \pm 1.0	...
		72	J153740.6+060316	15 37 40.6	+06 03 16	570	4.9	10.0 \pm 3.3	6.6 \pm 2.6	3.4 \pm 2.0	...
S3	S3	73	J153731.6+060316	15 37 31.6	+06 03 16	538	4.8	11.3 \pm 3.5	8.9 \pm 3.0	2.4 \pm 1.7	...
		74	J153724.7+060103	15 37 24.7	+06 01 03	585	3.6	5.0 \pm 2.2	0.0 \pm 0.0	5.0 \pm 2.2	...
		75	J153715.3+055908	15 37 15.3	+05 59 08	545	5.0	27.1 \pm 5.3	18.4 \pm 4.4	8.7 \pm 3.0	...
		76	J153714.8+055921	15 37 14.8	+05 59 21	543	5.2	12.5 \pm 3.6	6.7 \pm 2.7	5.8 \pm 2.5	...
		77	J153733.0+060350	15 37 33.0	+06 03 50	571	5.3	7.3 \pm 2.8	6.8 \pm 2.6	0.5 \pm 1.0	...
		78	J153725.3+060329	15 37 25.3	+06 03 29	566	5.5	17.2 \pm 4.2	9.6 \pm 3.2	7.6 \pm 2.8	...
		79	J153712.5+060053	15 37 12.5	+06 00 53	487	6.1	17.7 \pm 4.4	9.7 \pm 3.2	8.0 \pm 3.0	...
		80	J153708.2+060550	15 37 08.2	+06 05 50	514	9.9	57.8 \pm 8.0	40.1 \pm 6.5	17.7 \pm 4.6	...
		81	J153738.9+055845	15 37 38.9	+05 58 45	653	0.9	39.3 \pm 6.3	26.6 \pm 5.2	12.7 \pm 3.6	Y
		82	J153736.0+055545	15 37 36.0	+05 55 45	640	2.8	46.4 \pm 6.9	29.7 \pm 5.5	16.7 \pm 4.1	...
		83	J153733.1+055756	15 37 33.1	+05 57 56	650	0.8	23.5 \pm 4.9	16.8 \pm 4.1	6.7 \pm 2.6	Y
		84	J153737.3+055539	15 37 37.3	+05 55 39	614	2.9	11.6 \pm 3.5	8.8 \pm 3.0	2.8 \pm 1.7	...
		85	J153733.4+055915	15 37 33.4	+05 59 15	645	0.9	10.4 \pm 3.3	7.7 \pm 2.8	2.8 \pm 1.7	Y
		86	J153743.9+055632	15 37 43.9	+05 56 32	620	2.9	5.7 \pm 2.5	1.9 \pm 1.4	3.8 \pm 2.0	...
		87	J153750.5+055811	15 37 50.5	+05 58 11	629	3.8	10.3 \pm 3.3	6.7 \pm 2.6	3.7 \pm 2.0	...
		88	J153743.7+060104	15 37 43.7	+06 01 04	563	3.3	6.8 \pm 2.6	3.0 \pm 1.7	3.8 \pm 2.0	...
S4	S4	89	J153749.4+055832	15 37 49.4	+05 58 32	638	3.5	4.5 \pm 2.2	3.9 \pm 2.0	0.7 \pm 1.0	...
		90	J153752.8+055902	15 37 52.8	+05 59 02	622	4.4	10.4 \pm 3.5	8.3 \pm 3.0	2.0 \pm 1.7	...
		91	J153751.6+060003	15 37 51.6	+06 00 03	401	4.3	7.1 \pm 3.0	4.4 \pm 2.2	2.7 \pm 2.0	...
		92	J153730.8+055852	15 37 30.8	+05 58 52	644	1.2	4.9 \pm 2.2	1.0 \pm 1.0	4.0 \pm 2.0	Y
		93	J153758.4+054725	15 37 58.4	+05 47 25	498	12.5	18.2 \pm 6.5	18.4 \pm 5.3	-0.2 \pm 3.7	...

TABLE 3
CONTINUED

Obs ID	Chip Num	ID Num	Source Name (CXOU)	R.A. (J2000)	Decl. (J2000)	A_{eff} (cm 2)	Δ ($'$)	Net Counts \pm Error (0.3-8 keV)	Soft Counts \pm Error (0.3-2 keV)	Hard Counts \pm Error (2-8 keV)	Inside D25?
(1)	(2)	(3)	(4)	(5)	(6)	(7)	(8)	(9)	(10)	(11)	(12)
12983	S2	94	J112646.2+534921	11 26 46.2	+53 49 21	555	4.6	65.2 \pm 8.1	40.8 \pm 6.4	24.4 \pm 5.0	...
		95	J112622.4+534722	11 26 22.4	+53 47 22	586	3.5	9.8 \pm 3.2	6.0 \pm 2.4	3.8 \pm 2.0	...
		96	J112632.0+535022	11 26 32.0	+53 50 22	522	5.6	9.4 \pm 3.2	7.9 \pm 2.8	1.5 \pm 1.4	...
		97	J112629.1+535007	11 26 29.1	+53 50 07	469	5.4	8.5 \pm 3.0	6.9 \pm 2.6	1.7 \pm 1.4	...
		98	J112626.1+534955	11 26 26.1	+53 49 55	479	5.4	9.6 \pm 3.2	9.9 \pm 3.2	-0.3 \pm 0.1	...
		99	J112623.5+534855	11 26 23.5	+53 48 55	542	4.7	7.6 \pm 2.8	5.0 \pm 2.2	2.7 \pm 1.7	...
		100	J112606.4+534857	11 26 06.4	+53 48 57	434	6.3	18.7 \pm 4.5	10.5 \pm 3.3	8.2 \pm 3.0	...
		101	J112656.1+533932	11 26 56.1	+53 39 32	612	5.9	24.6 \pm 5.1	18.5 \pm 4.4	6.1 \pm 2.7	...
		102	J112659.2+534517	11 26 59.2	+53 45 17	612	3.0	13.7 \pm 3.7	10.9 \pm 3.3	2.8 \pm 1.7	...
		103	J112642.2+534258	11 26 42.2	+53 42 58	650	2.0	7.6 \pm 2.8	7.9 \pm 2.8	-0.2 \pm 0.1	...
12984	S3	104	J112635.7+534456	11 26 35.7	+53 44 56	649	0.5	4.7 \pm 2.2	3.8 \pm 2.0	1.0 \pm 1.0	Y
		105	J112626.7+534437	11 26 26.7	+53 44 37	641	1.9	6.3 \pm 2.7	5.8 \pm 2.5	0.5 \pm 1.0	...
		106	J112620.9+534447	11 26 20.9	+53 44 47	630	2.7	8.8 \pm 3.0	6.0 \pm 2.4	2.9 \pm 1.7	...
		107	J112654.6+534002	11 26 54.6	+53 40 02	621	5.4	12.5 \pm 3.8	3.3 \pm 2.0	9.1 \pm 3.2	...
		108	J112645.6+533911	11 26 45.6	+53 39 11	613	5.8	25.7 \pm 5.2	19.5 \pm 4.5	6.1 \pm 2.7	...
		109	J112717.0+534112	11 27 17.0	+53 41 12	593	6.7	14.4 \pm 4.3	9.7 \pm 3.3	4.7 \pm 2.7	...
		110	J092044.7+641042	09 20 44.7	+64 10 42	574	5.2	11.7 \pm 3.5	9.0 \pm 3.0	2.7 \pm 1.7	...
		111	J092038.2+641429	09 20 38.2	+64 14 29	535	8.4	18.2 \pm 4.5	13.6 \pm 3.7	4.7 \pm 2.5	...
		112	J092037.0+641349	09 20 37.0	+64 13 49	542	7.8	7.5 \pm 3.2	6.3 \pm 2.7	1.2 \pm 1.8	...
		113	J092020.6+640607	09 20 20.6	+64 06 07	655	0.2	4.6 \pm 2.2	3.9 \pm 2.0	0.8 \pm 1.0	Y
S4	S3	114	J092019.5+640454	09 20 19.5	+64 04 54	652	1.4	37.4 \pm 6.2	21.8 \pm 4.7	15.7 \pm 4.0	Y
		115	J092013.7+640606	09 20 13.7	+64 06 06	618	0.6	95.7 \pm 9.8	62.9 \pm 7.9	32.8 \pm 5.7	Y
		116	J092006.3+640738	09 20 06.3	+64 07 38	640	1.9	102.8 \pm 10.1	79.0 \pm 8.9	23.9 \pm 4.9	Y
		117	J092021.0+640617	09 20 21.0	+64 06 17	654	0.2	6.6 \pm 2.6	3.8 \pm 2.0	2.8 \pm 1.7	Y
		118	J092019.5+640624	09 20 19.5	+64 06 24	653	0.1	8.6 \pm 3.0	6.8 \pm 2.6	1.8 \pm 1.4	Y
		119	J092018.6+640615	09 20 18.6	+64 06 15	654	0.1	12.5 \pm 3.6	6.9 \pm 2.6	5.7 \pm 2.5	Y
		120	J092014.9+640436	09 20 14.9	+64 04 36	650	1.8	24.6 \pm 5.0	18.8 \pm 4.4	5.9 \pm 2.5	Y
		121	J092013.1+640440	09 20 13.1	+64 04 40	650	1.8	7.7 \pm 2.8	6.9 \pm 2.6	0.9 \pm 1.0	Y
		122	J092034.5+640643	09 20 34.5	+64 06 43	647	1.7	5.5 \pm 2.5	4.8 \pm 2.2	0.7 \pm 1.0	Y
		123	J092033.2+640345	09 20 33.2	+64 03 45	639	3.0	8.6 \pm 3.0	6.7 \pm 2.6	1.9 \pm 1.4	Y
		124	J092032.1+640424	09 20 32.1	+64 04 24	651	2.4	9.7 \pm 3.2	4.9 \pm 2.2	4.8 \pm 2.2	Y
		125	J092020.2+640409	09 20 20.2	+64 04 09	646	2.2	4.5 \pm 2.2	1.7 \pm 1.4	2.8 \pm 1.7	Y
		126	J092011.2+640723	09 20 11.2	+64 07 23	645	1.4	9.6 \pm 3.2	8.8 \pm 3.0	0.8 \pm 1.0	Y
		127	J091947.6+640743	09 19 47.6	+64 07 43	606	3.7	18.8 \pm 4.4	6.0 \pm 2.4	12.9 \pm 3.6	...
		128	J091957.5+640206	09 19 57.5	+64 02 06	599	4.8	10.8 \pm 3.5	5.5 \pm 2.5	5.2 \pm 2.5	...
		129	J092043.5+640052	09 20 43.5	+64 00 52	580	6.1	16.3 \pm 4.5	8.6 \pm 3.2	7.7 \pm 3.2	...
		130	J091953.3+640337	09 19 53.3	+64 03 37	628	3.9	5.7 \pm 2.5	3.9 \pm 2.0	1.8 \pm 1.4	...
		131	J091946.9+635717	09 19 46.9	+63 57 17	527	9.7	23.7 \pm 5.4	18.8 \pm 4.6	4.9 \pm 2.9	...
		132	J092037.7+635827	09 20 37.7	+63 58 27	357	8.1	20.3 \pm 4.6	10.8 \pm 3.3	9.4 \pm 3.2	...
		133	J091955.4+635934	09 19 55.4	+63 59 34	406	7.2	14.7 \pm 4.0	7.4 \pm 2.8	7.2 \pm 2.8	...
		134	J092004.9+635528	09 20 04.9	+63 55 28	399	10.9	30.4 \pm 5.9	20.4 \pm 4.7	10.0 \pm 3.6	...
		135	J091944.8+635739	09 19 44.8	+63 57 39	530	9.4	13.8 \pm 4.4	4.0 \pm 2.5	9.8 \pm 3.6	...

TABLE 3
CONTINUED

Obs ID	Chip Num	ID Num	Source Name (CXOU)	R.A. (J2000)	Decl. (J2000)	A_{eff} (cm^2)	Δ (')	Net Counts \pm Error (0.3-8 keV)	Soft Counts \pm Error (0.3-2 keV)	Hard Counts \pm Error (2-8 keV)	Inside D25?
(1)	(2)	(3)	(4)	(5)	(6)	(7)	(8)	(9)	(10)	(11)	(12)
12985	S2	136	J103535.3-244318	10 35 35.3	-24 43 18	563	3.3	26.9 \pm 5.2	19.9 \pm 4.5	7.0 \pm 2.6	...
		137	J103510.4-243846	10 35 10.4	-24 38 46	482	6.7	47.8 \pm 7.0	27.7 \pm 5.3	20.1 \pm 4.6	...
		138	J103514.5-243939	10 35 14.5	-24 39 39	562	5.6	6.8 \pm 2.6	4.9 \pm 2.2	1.9 \pm 1.4	...
		139	J103507.0-244149	10 35 07.0	-24 41 49	549	4.7	7.6 \pm 2.8	3.9 \pm 2.0	3.7 \pm 2.0	...
		140	J103520.7-243708	10 35 20.7	-24 37 08	540	7.8	14.4 \pm 4.0	11.5 \pm 3.5	2.9 \pm 2.0	...
	S3	141	J103522.2-244513	10 35 22.2	-24 45 13	653	0.3	867.0 \pm 29.5	528.7 \pm 23.0	338.3 \pm 18.4	Y
		142	J103523.3-244517	10 35 23.3	-24 45 17	654	0.4	68.3 \pm 8.3	40.7 \pm 6.4	27.6 \pm 5.3	Y
		143	J103526.9-244745	10 35 26.9	-24 47 45	602	3.0	7.6 \pm 2.8	6.7 \pm 2.6	0.9 \pm 1.0	...
		144	J103522.8-244632	10 35 22.8	-24 46 32	651	1.6	8.5 \pm 3.0	8.8 \pm 3.0	-0.3 \pm 0.1	Y
		145	J103522.6-244503	10 35 22.6	-24 45 03	653	0.2	17.7 \pm 4.4	11.5 \pm 3.5	6.2 \pm 2.7	Y
12986	S2	146	J103514.8-244455	10 35 14.8	-24 44 55	644	1.8	8.5 \pm 3.0	6.8 \pm 2.6	1.8 \pm 1.4	...
		147	J103534.2-244448	10 35 34.2	-24 44 48	641	2.6	8.5 \pm 3.0	7.0 \pm 2.6	1.5 \pm 1.4	...
		148	J103529.5-244835	10 35 29.5	-24 48 35	634	4.0	7.5 \pm 3.0	5.7 \pm 2.5	1.8 \pm 1.7	...
		149	J103528.3-244824	10 35 28.3	-24 48 24	634	3.7	5.8 \pm 2.5	3.0 \pm 1.7	2.8 \pm 1.7	...
		150	J103503.4-244814	10 35 03.4	-24 48 14	337	5.5	23.3 \pm 4.9	16.5 \pm 4.1	6.7 \pm 2.7	...
	S3	151	J103511.5-245055	10 35 11.5	-24 50 55	603	6.5	19.0 \pm 4.8	12.8 \pm 3.7	6.2 \pm 3.0	...
		152	J103509.4-245248	10 35 09.4	-24 52 48	540	8.5	18.0 \pm 4.5	12.0 \pm 3.6	6.0 \pm 2.7	...
		153	J103528.1-245347	10 35 28.1	-24 53 47	537	9.0	21.0 \pm 5.2	11.2 \pm 3.6	9.8 \pm 3.8	...
		154	J114109.6+561522	11 41 09.6	+56 15 22	586	4.0	4.3 \pm 2.2	0.7 \pm 1.0	3.6 \pm 2.0	...
		155	J114054.5+561557	11 40 54.5	+56 15 57	588	3.8	4.8 \pm 2.2	3.0 \pm 1.7	1.9 \pm 1.4	...
S4	S2	156	J114048.5+561847	11 40 48.5	+56 18 47	500	6.6	14.4 \pm 4.0	10.5 \pm 3.3	4.0 \pm 2.2	...
		157	J114033.8+561520	11 40 33.8	+56 15 20	557	4.1	4.3 \pm 2.2	2.8 \pm 1.7	1.5 \pm 1.4	...
		158	J114050.2+561708	11 40 50.2	+56 17 08	575	5.0	7.5 \pm 2.8	0.9 \pm 1.0	6.7 \pm 2.6	...
		159	J114053.5+561011	11 40 53.5	+56 10 11	649	2.0	22.6 \pm 4.8	13.9 \pm 3.7	8.7 \pm 3.0	...
		160	J114047.6+561059	11 40 47.6	+56 10 59	649	1.3	6.7 \pm 2.6	4.9 \pm 2.2	1.9 \pm 1.4	...
		161	J114038.0+561023	11 40 38.0	+56 10 23	637	2.6	14.6 \pm 3.9	11.0 \pm 3.3	3.7 \pm 2.0	...
		162	J114119.6+561258	11 41 19.6	+56 12 58	625	3.9	10.8 \pm 3.3	8.9 \pm 3.0	1.9 \pm 1.4	...
	S3	163	J114112.4+561441	11 41 12.4	+56 14 41	179	3.8	8.8 \pm 3.0	9.0 \pm 3.0	-0.2 \pm 0.1	...
		164	J114109.7+560819	11 41 09.7	+56 08 19	630	4.6	60.1 \pm 7.8	54.8 \pm 7.4	5.3 \pm 2.5	...
		165	J114104.4+561238	11 41 04.4	+56 12 38	651	1.8	7.9 \pm 2.8	3.9 \pm 2.0	4.0 \pm 2.0	...
		166	J114035.5+560914	11 40 35.5	+56 09 14	622	3.7	22.7 \pm 4.8	14.8 \pm 3.9	7.9 \pm 2.8	...
		167	J114053.4+560809	11 40 53.4	+56 08 09	633	4.0	17.1 \pm 4.2	12.7 \pm 3.6	4.4 \pm 2.2	...
		168	J114119.0+560932	11 41 19.0	+56 09 32	627	4.6	9.3 \pm 3.3	7.9 \pm 3.0	1.4 \pm 1.4	...
		169	J114115.4+560841	11 41 15.4	+56 08 41	630	4.7	5.9 \pm 2.7	2.6 \pm 1.7	3.3 \pm 2.0	...
S4	S2	170	J114114.8+561409	11 41 14.8	+56 14 09	580	3.7	4.7 \pm 2.2	3.9 \pm 2.0	0.9 \pm 1.0	...
		171	J114129.8+560732	11 41 29.8	+56 07 32	593	7.0	28.5 \pm 5.8	31.0 \pm 5.8	-2.4 \pm 0.3	...
		172	J114124.3+560449	11 41 24.3	+56 04 49	460	8.6	15.5 \pm 4.6	13.4 \pm 3.9	2.1 \pm 2.5	...
		173	J114049.3+560101	11 40 49.3	+56 01 01	493	11.2	71.2 \pm 8.7	48.5 \pm 7.1	22.7 \pm 5.1	...
		174	J114118.4+560248	11 41 18.4	+56 02 48	525	10.1	9.1 \pm 3.8	5.4 \pm 2.7	3.8 \pm 2.7	...

NOTE. — Column 1: The *Chandra* observation ID of the exposure that found this source, as well as the target galaxy of that observation. Column 2: The ACIS-S chip that this source was observed on. Column 3: Assigned ID number of the source. Column 4: Chandra ID name. Columns 5, 6: R.A. and Decl. of source in the J2000 epoch. Column 7: The 1.7 keV effective area at the location of the source. This is the net instrument response, integrated over the dither path of the observation. Sources with lower effective areas are typically on CCD chip edges. Column 8: Angular distance from the pointing location of the observation to the source, in arcminutes. Columns 9, 10, 11: Background subtracted net counts, with 1σ uncertainties, in broad (0.3-8 keV), soft (0.3-2 keV) and hard (2-8 keV) bands respectively. Column 12: Is this object within the D25 isophote of the target galaxy? "Y" if yes, "..." if no.

TABLE 4
USNO–B1.0 CROSS CORRELATION

N (1)	Source Name (2)	Identification (USNO–B1.0) (3)	Δ ($''$) (4)	B1 (mag) (5)	R1 (mag) (6)	B2 (mag) (7)	R2 (mag) (8)	I (mag) (9)	R.A. (B1.0) (10)	Decl. (B1.0) (11)	α (mas/yr) (12)	δ (mas/yr) (13)
1	79.6.01	0824–0013640	0.68	19.1	19.31	19.76	19.65	18.61	00 59 51.705	−07 30 52.15	0	0
12	79.7.09	0824–0013616	1.06		18.26			16.17	00 59 47.553	−07 34 15.91	0	0
13	79.7.10	0824–0013575	0.12	21.3	19.3	21.81	20.14	18.7	00 59 40.451	−07 33 47.90	0	0
14	79.7.11	0824–0013656	1.46	17.81			18.66	18.59	00 59 53.323	−07 35 22.20	−62	4
16	79.7.13	0823–0014391	1.66	15.88	15.48	15.89	14.37	13.61	00 59 48.055	−07 38 06.60	4	−4
20	79.7.17	0823–0014409	0.9				20.32	18.71	00 59 56.411	−07 38 32.72	0	0
21	79.7.19	0823–0014364	0.83	20.6		20.83	20.31		00 59 35.397	−07 36 21.56	0	0
31	80.7.01	1393–0289816	0.13	20.2	19.56	20.98	20.17		18 34 02.167	+49 18 17.09	0	0
32	80.7.02	1392–0289637	0.53	19.17		16.81	18.73		18 33 55.789	+49 17 46.10	4	−58
35	80.7.05	1392–0289517	0.1		20.14	20.9	20.16		18 33 33.403	+49 16 17.55	12	−2
38	80.7.08	1392–0289633	0.65	17.81	18.13	16.36	17.92		18 33 55.458	+49 17 41.16	0	0
39	80.7.09	1392–0289563	0.67	14.28	13.29	13.7	12.74	12.61	18 33 46.081	+49 17 11.49	2	−30
40	80.7.10	1392–0289720	0.47	21.15	19.31	21.13	19.74	18.53	18 34 15.721	+49 12 42.37	0	0
44	80.7.14	1392–0289503	0.92	10.95	9.41	10.39	9.36	8.93	18 33 31.785	+49 14 17.00	4	2
45	80.7.15	1392–0289498	1.59		19.99	21.59			18 33 30.913	+49 12 15.28	0	0
51	81.6.05	0838–0010164	1.17	18.77	19.3	18.79	18.66	18.36	01 04 42.205	−06 07 10.69	0	0
72	82.6.03	0960–0249967	0.89	20.93		21.62			15 37 40.591	+06 03 16.07	0	0
75	82.6.06	0959–0250209	1.06	20.45		20.63	20.11	18.53	15 37 15.377	+05 59 06.94	0	0
80	82.6.11	0960–0249848	0.75	20.3		20.57	19.98	18.75	15 37 08.145	+06 05 49.62	0	0
85	82.7.05	0959–0250298	1.34		19.12	19.03			15 37 33.448	+05 59 15.95	0	0
93	82.8.02	0957–0253217	1.78	18.04	15.25	17.34	15.21	13.39	15 37 58.309	+05 47 24.96	10	−62
94	83.6.01	1438–0211891	0.45	20.44		21.54	20.36		11 26 46.228	+53 49 21.66	0	0
96	83.6.04	1438–0211867	0.78	20.22	19.56	19.99	20.11	18.65	11 26 31.999	+53 50 22.97	0	0
98	83.6.06	1438–0211856	1.02	20.86		20.92			11 26 26.220	+53 49 55.10	0	0
100	83.6.08	1438–0211831	1.68	20.81		21.1			11 26 06.327	+53 48 58.98	0	0
101	83.7.01	1436–0212315	0.59	20.97	20.15	20.78			11 26 56.012	+53 39 31.98	0	0
108	83.7.08	1436–0212295	0.23	20.1	19.55	19.92	20.38		11 26 45.612	+53 39 11.16	0	0
114	84.7.02	1540–0162426	1.44		17.45	17.97			09 20 19.686	+64 04 54.90	0	0
115	84.7.03	1541–0161956	0.38	19.7		15.9			09 20 13.644	+64 06 05.66	0	0
121	84.7.09	1540–0162375	0.49	16.52		15.2			09 20 13.090	+64 04 39.26	0	0
122	84.7.10	1541–0162121	1.92	18.77		18.62			09 20 34.450	+64 06 41.57	0	0
126	84.7.14	1541–0161927	0.81	20.11	16.86	20.17	17.63	15.74	09 20 11.188	+64 07 24.10	−16	−14
129	84.7.18	1540–0162548	0.36		19.53	21.36			09 20 43.530	+64 00 52.01	0	0
131	84.8.01	1539–0165598	1.53	19.85	19.53	20.48	19.66	18.6	09 19 47.112	+63 57 16.34	0	0
132	84.8.02	1539–0165727	0.28	20.12	19.56	21.39			09 20 37.692	+63 58 27.54	0	0
134	84.8.04	1539–0165649	1.46	19.1	19.38	19.62	18.96	18.56	09 20 04.903	+63 55 26.45	−12	12
136	85.6.01	0652–0248014	0.76	19.61	18.74	20.12	18.9		10 35 35.286	−24 43 18.09	0	0
142	85.7.01	0652–0247945	0.9	15.42	16.33	11.9	16.99	16.65	10 35 23.305	−24 45 17.45	10	−60
	85.7.01	0652–0247946	1.42	15.41	16.33		13.86	16.61	10 35 23.307	−24 45 15.14	0	0
144	85.7.05	0652–0247936	0.08	16.41	14.24	16.24	14.27	13.6	10 35 22.787	−24 46 31.55	0	0
164	86.7.07	1461–0224874	0.61	20.42	18.22	19.56	18.32	15.91	11 41 09.618	+56 08 19.10	0	0
166	86.7.10	1461–0224784	0.5	20.85		21.6			11 40 35.478	+56 09 14.25	0	0
171	86.7.15	1461–0224928	1.07	12.79	10.95	12.09	10.89	10.39	11 41 29.713	+56 07 32.05	−142	8
172	86.8.01	1460–0217838	0.4	20.53	20.27	20.54	20.72		11 41 24.294	+56 04 48.86	0	0

NOTE. — Column 1: Source number from Table 4. Column 2: Observation ID, CCD chip number, and WAVDETECT source number. Column 3: Identification number for the identified USNO–B1.0 source. Column 4: Offset between X-ray source and USNO–B1.0 source centroids. Column 5–9: First and second B and R magnitudes, and I magnitudes, for each source. Typical errors are 0.3 mag. Column 10–11: R.A. and Decl. of the source listed in USNO–B1.0 catalog. Column 12–13: Proper motion of the source.

TABLE 5
SDSS DR8 CROSS CORRELATION

N	Source Name	Identification (SDSS DR8)	Δ ('')	u (mag)	g (mag)	r (mag)	i (mag)	z (mag)	R.A. (SDSS)	Decl. (SDSS)	cl
(1)	(2)	(3)	(4)	(5)	(6)	(7)	(8)	(9)	(10)	(11)	(12)
1	79.6.01	J005951.73-073052.1	0.325	20.064 (± 0.054)	19.807 (± 0.016)	19.523 (± 0.016)	19.503 (± 0.02)	19.316 (± 0.06)	00 59 51.734	-07 30 52.16	6
9	79.7.06	J005949.48-073522.8	0.584	16.471 (± 0.068)	14.233 (± 0.004)	13.956 (± 0.005)	13.744 (± 0.006)	14.041 (± 0.026)	00 59 49.482	-07 35 22.89	3
12	79.7.09	J005947.49-073416.0	0.556	20.181 (± 0.075)	20.101 (± 0.028)	20.305 (± 0.039)	20.833 (± 0.078)	21.287 (± 0.41)	00 59 47.499	-07 34 16.02	3
13	79.7.10	J005940.46-073348.1	0.308	23.009 (± 0.735)	21.504 (± 0.076)	20.189 (± 0.037)	19.648 (± 0.033)	19.225 (± 0.087)	00 59 40.464	-07 33 48.19	3
16	79.7.13	J005948.10-073808.1	0.107	19.459 (± 0.037)	16.958 (± 0.004)	15.761 (± 0.004)	15.215 (± 0.004)	14.875 (± 0.005)	00 59 48.103	-07 38 08.19	6
17	79.7.14	J005954.59-073656.2	0.548	22.646 (± 0.649)	23.19 (± 0.314)	22.006 (± 0.185)	21.437 (± 0.168)	21.635 (± 0.776)	00 59 54.590	-07 36 56.25	3
20	79.7.17	J005956.43-073832.3	0.495	22.734 (± 0.685)	21.67 (± 0.083)	20.404 (± 0.046)	19.815 (± 0.041)	19.37 (± 0.112)	00 59 56.433	-07 38 32.36	3
21	79.7.19	J005935.40-073621.5	0.872	25.23 (± 1.213)	20.934 (± 0.033)	20.492 (± 0.034)	20.394 (± 0.043)	20.055 (± 0.132)	00 59 35.404	-07 36 21.56	6
49	81.6.03	J010454.29-060621.0	1.315	24.5 (± 0.995)	22.252 (± 0.102)	22.182 (± 0.109)	22.364 (± 0.189)	22.626 (± 0.536)	01 04 54.295	-06 06 21.02	6
51	81.6.05	J010442.22-060710.7	1.154	19.475 (± 0.033)	19.035 (± 0.01)	18.79 (± 0.01)	18.503 (± 0.01)	18.476 (± 0.026)	01 04 42.224	-06 07 10.75	6
56	81.7.05	J010513.94-061028.6	0.791	21.965 (± 0.247)	22.012 (± 0.082)	21.627 (± 0.092)	21.341 (± 0.111)	21.049 (± 0.3)	01 05 13.946	-06 10 28.69	6
58	81.7.08	J010516.08-061748.1	0.464	25.887 (± 1.083)	21.41 (± 0.06)	20.867 (± 0.061)	20.13 (± 0.047)	19.792 (± 0.123)	01 05 16.086	-06 17 48.13	3
61	81.7.11	J010522.28-061151.4	1.35	23.002 (± 0.587)	21.638 (± 0.059)	21.479 (± 0.078)	21.393 (± 0.112)	21.301 (± 0.352)	01 05 22.288	-06 11 51.45	6
62	81.7.12	J010515.53-061639.9	0.906	25.7 (± 1.235)	23.658 (± 0.405)	21.5 (± 0.105)	20.853 (± 0.088)	20.385 (± 0.21)	01 05 15.538	-06 16 39.96	3
63	81.7.13	J010523.59-061249.6	1.864	23.448 (± 0.871)	22.171 (± 0.095)	22.35 (± 0.173)	22.26 (± 0.244)	21.693 (± 0.493)	01 05 23.591	-06 12 49.68	6
67	81.8.01	J010529.70-061733.4	1.035	23.636 (± 1.049)	22.658 (± 0.146)	22.177 (± 0.157)	21.793 (± 0.161)	21.034 (± 0.287)	01 05 29.708	-06 17 33.42	6
69	81.8.03	J010513.11-062151.9	1.416	22.193 (± 0.353)	21.983 (± 0.086)	21.427 (± 0.084)	21.421 (± 0.132)	21.36 (± 0.47)	01 05 13.116	-06 21 51.98	3
72	82.6.03	J153740.62+060315.9	0.395	21.92 (± 0.607)	21.359 (± 0.179)	21.137 (± 0.152)	20.947 (± 0.151)	20.675 (± 0.296)	15 37 40.625	+06 03 15.99	3
75	82.6.06	J153715.37+055906.9	1.043	20.785 (± 0.094)	20.138 (± 0.021)	19.84 (± 0.023)	19.459 (± 0.022)	19.438 (± 0.072)	15 37 15.378	+05 59 06.98	6
78	82.6.09	J153725.35+060329.7	0.698	21.084 (± 3.902)	30.972 (± 0.282)	30.144 (± 0.514)	17.354 (± 0.113)	27.633 (± 0.777)	15 37 25.350	+06 03 29.71	3
79	82.6.10	J153712.43+060053.8	0.888	24.473 (± 1.854)	22.594 (± 0.205)	21.717 (± 0.142)	21.073 (± 0.115)	20.463 (± 0.238)	15 37 12.438	+06 00 53.85	3
80	82.6.11	J153708.14+060549.3	0.947	20.671 (± 0.058)	20.489 (± 0.021)	20.305 (± 0.025)	20.102 (± 0.033)	19.822 (± 0.09)	15 37 08.148	+06 05 49.38	6
84	82.7.04	J153737.26+055538.7	0.149	22.839 (± 0.374)	22.261 (± 0.102)	21.799 (± 0.092)	21.484 (± 0.112)	22.117 (± 0.647)	15 37 37.264	+05 55 38.79	6
89	82.7.09	J153749.45+055832.7	1.311	23.339 (± 0.538)	22.196 (± 0.091)	22.129 (± 0.129)	22.266 (± 0.241)	22.491 (± 0.734)	15 37 49.454	+05 58 32.73	6
90	82.7.10	J153752.79+055902.5	0.125	23.847 (± 0.58)	22.653 (± 0.109)	21.497 (± 0.06)	21.115 (± 0.071)	20.793 (± 0.192)	15 37 52.790	+05 59 02.57	6
93	82.8.02	J153758.31+054724.7	1.716	19.989 (± 0.039)	17.179 (± 0.005)	15.643 (± 0.004)	13.944 (± 0.004)	12.994 (± 0.004)	15 37 58.311	+05 47 24.70	6
94	83.6.01	J112646.20+534921.7	0.392	20.508 (± 0.063)	20.963 (± 0.032)	20.494 (± 0.031)	20.479 (± 0.042)	20.473 (± 0.154)	11 26 46.202	+53 49 21.74	6
95	83.6.03	J112622.35+534723.6	1.457	23.626 (± 0.888)	24.61 (± 0.65)	24.062 (± 0.7)	22.166 (± 0.238)	22.098 (± 0.726)	11 26 22.355	+53 47 23.63	3
96	83.6.04	J112631.99+535023.0	0.899	20.957 (± 0.078)	19.764 (± 0.014)	19.548 (± 0.018)	19.481 (± 0.021)	19.765 (± 0.086)	11 26 31.998	+53 50 23.09	6
97	83.6.05	J112629.22+535007.3	1.006	26.147 (± 0.614)	22.885 (± 0.219)	21.513 (± 0.122)	20.412 (± 0.062)	19.791 (± 0.137)	11 26 29.228	+53 50 07.32	3
98	83.6.06	J112626.22+534955.1	1.085	22.182 (± 0.219)	20.872 (± 0.031)	20.786 (± 0.049)	21.014 (± 0.077)	20.437 (± 0.168)	11 26 26.225	+53 49 55.17	6
99	83.6.07	J112623.54+534856.6	1.297	22.806 (± 0.44)	21.983 (± 0.081)	21.934 (± 0.116)	21.527 (± 0.118)	20.889 (± 0.263)	11 26 23.549	+53 48 56.66	6
101	83.7.01	J112656.08+533923.3	0.205	24.093 (± 1.048)	21.935 (± 0.075)	21.59 (± 0.084)	21.617 (± 0.121)	20.738 (± 0.218)	11 26 56.083	+53 39 32.36	6
102	83.7.02	J112659.25+534517.1	0.6	21.991 (± 0.22)	21.757 (± 0.066)	21.824 (± 0.101)	21.244 (± 0.089)	21.367 (± 0.358)	11 26 59.252	+53 45 17.19	6
103	83.7.03	J112641.96+534258.5	1.948	14.521 (± 0.007)	10.832 (± 0.001)	9.905 (± 0.001)	9.716 (± 0.001)	9.823 (± 0.001)	11 26 41.965	+53 42 58.59	6
108	83.7.08	J112645.63+533911.3	0.242	20.243 (± 0.052)	20.15 (± 0.019)	20.051 (± 0.023)	19.891 (± 0.026)	19.809 (± 0.09)	11 26 45.636	+53 39 11.31	6
112	84.6.03	J092036.88+641348.9	0.679	23.334 (± 0.754)	22.584 (± 0.133)	22.435 (± 0.22)	21.725 (± 0.184)	21.101 (± 0.356)	09 20 36.885	+64 13 48.95	3
115	84.7.03	J092013.63+640605.4	0.65	20.158 (± 0.058)	20.149 (± 0.021)	20.156 (± 0.028)	20.439 (± 0.054)	20.6 (± 0.232)	09 20 13.635	+64 06 05.40	6
118	84.7.06	J092019.51+640622.3	1.235	21.442 (± 0.167)	21.442 (± 0.064)	21.642 (± 0.114)	21.742 (± 0.196)	22.827 (± 0.987)	09 20 19.511	+64 06 22.35	6
119	84.7.07	J092018.87+640615.2	1.804	22.74 (± 0.463)	23.664 (± 0.367)	22.382 (± 0.18)	24.233 (± 0.884)	22.827 (± 0.828)	09 20 18.878	+64 06 15.20	6
124	84.7.12	J092032.26+640422.2	1.807	20.452 (± 0.074)	19.886 (± 0.017)	19.926 (± 0.024)	20.518 (± 0.061)	20.111 (± 0.161)	09 20 32.267	+64 04 22.26	3
126	84.7.14	J092011.17+640724.0	0.739	24.147 (± 1.043)	20.063 (± 0.017)	18.452 (± 0.009)	17.06 (± 0.006)	16.318 (± 0.008)	09 20 11.176	+64 07 24.01	6
129	84.7.18	J092043.52+640050.5	1.09	21.431 (± 0.14)	21.782 (± 0.062)	21.272 (± 0.064)	21.27 (± 0.103)	21.269 (± 0.389)	09 20 43.523	+64 00 50.57	6
130	84.7.19	J091953.27+640336.7	0.384	24.146 (± 0.993)	23.535 (± 0.245)	21.945 (± 0.104)	21.661 (± 0.136)	21.517 (± 0.454)	09 19 53.272	+64 03 36.75	6
131	84.8.01	J091947.13+635716.3	1.649	20.277 (± 0.052)	20.146 (± 0.018)	19.876 (± 0.02)	19.895 (± 0.029)	19.879 (± 0.112)	09 19 47.130	+63 57 16.35	6
132	84.8.02	J092037.69+635827.5	0.298	22.358 (± 0.284)	21.915 (± 0.063)	21.645 (± 0.078)	20.965 (± 0.07)	20.397 (± 0.167)	09 20 37.695	+63 58 27.55	6

TABLE 5
CONTINUED

N	Source Name	Identification (SDSS DR8)	Δ ('')	u (mag)	g (mag)	r (mag)	i (mag)	z (mag)	R.A. (SDSS)	Decl. (SDSS)	cl
(1)	(2)	(3)	(4)	(5)	(6)	(7)	(8)	(9)	(10)	(11)	(12)
133	84.8.03	J091955.38+635934.5	0.135	23.64 (± 0.774)	22.558 (± 0.111)	21.916 (± 0.15)	21.392 (± 0.105)	20.792 (± 0.268)	09 19 55.386	+63 59 34.54	3
134	84.8.04	J092004.93+635526.3	1.557	20.015 (± 0.044)	19.765 (± 0.014)	19.441 (± 0.015)	19.416 (± 0.02)	19.391 (± 0.073)	09 20 04.939	+63 55 26.37	6
154	86.6.02	J114109.68+561523.3	1.115	23.238 (± 0.603)	22.78 (± 0.189)	22.084 (± 0.156)	21.101 (± 0.108)	20.482 (± 0.217)	11 41 09.680	+56 15 23.34	3
160	86.7.02	J114047.66+561059.0	0.434	27.663 (± 0.949)	29.494 (± 0.203)	19.648 (± 0.119)	20.029 (± 0.287)	20.685 (± 1.984)	11 40 47.665	+56 10 59.06	3
163	86.7.06	J114112.36+561441.2	0.326	22.09 (± 0.212)	22.112 (± 0.095)	21.51 (± 0.084)	21.329 (± 0.116)	21.137 (± 0.335)	11 41 12.362	+56 14 41.20	6
164	86.7.07	J114109.64+560818.9	0.362	22.11 (± 0.215)	19.829 (± 0.016)	18.446 (± 0.008)	17.227 (± 0.006)	16.498 (± 0.009)	11 41 09.643	+56 08 18.97	6
165	86.7.08	J114104.40+561237.6	0.132	22.119 (± 0.219)	22.832 (± 0.174)	22.833 (± 0.26)	22.871 (± 0.433)	21.866 (± 0.58)	11 41 04.409	+56 12 37.68	6
166	86.7.10	J114035.56+560914.6	0.346	21.404 (± 0.121)	21.242 (± 0.046)	21.513 (± 0.08)	21.411 (± 0.122)	21.102 (± 0.332)	11 40 35.563	+56 09 14.67	6
171	86.7.15	J114129.64+560732.3	1.685	15.158 (± 0.005)	12.543 (± 0.001)	11.221 (± 0.001)	10.815 (± 0.001)	12.496 (± 0.008)	11 41 29.643	+56 07 32.32	6
172	86.8.01	J114124.27+560448.9	0.386	20.928 (± 0.08)	20.981 (± 0.038)	20.623 (± 0.041)	20.661 (± 0.066)	20.377 (± 0.18)	11 41 24.277	+56 04 48.99	6
173	86.8.02	J114049.13+560101.7	1.449	20.581 (± 0.062)	20.259 (± 0.022)	20.124 (± 0.024)	20.101 (± 0.033)	19.781 (± 0.09)	11 40 49.139	+56 01 01.77	6

NOTE. — This table is the result of a cross-correlation between Table 3 and the Sloan Digital Sky Survey Data Release 8 point source catalog. IC 1291 and ESO 501-23 are not in the Sloan footprint, so none of these sources have SDSS counterparts. Column 1: Source number from Table 4. Column 2: Observation ID, CCD chip number, and WAVDETECT source number. Column 3: Identification number for the identified SDSS DR8 source. Column 4: Offset between centroid of *Chandra* and SDSS DR8 sources. Columns 5-9: Magnitudes for each of the five Sloan Digital Sky Survey band passes (ugriz), with errors. Columns 10-11: R.A. and Decl. of the SDSS DR8 source, in the J2000 epoch. Column 12: Object class listed in the SDSS DR8 catalog. 3 stands for galaxy, whereas 6 stands for star.

TABLE 6
WISE CROSS CORRELATION

N	Source Name	Identification (WISE)	Δ ('')	W1 (mag)	W2 (mag)	W3 (mag)	W4 (mag)	R.A. (WISE)	Decl. (WISE)
(1)	(2)	(3)	(4)	(5)	(6)	(7)	(8)	(9)	(10)
1	79.6.01	J005951.71-073052.0	0.476	15.564 (± 0.053)	14.223 (± 0.068)	12.155 (± 0.459)	>8.73	00 59 51.718	-07 30 52.08
3	79.6.03	J005944.62-073059.1	1.766	17.297 (± 0.212)	16.096 (± 0.308)	12.096 (± 0.461)	>8.169	00 59 44.623	-07 30 59.13
7	79.7.04	J005950.64-073457.1	1.525	11.578 (± 0.022)	11.277 (± 0.023)	6.762 (± 0.015)	3.742 (± 0.019)	00 59 50.646	-07 34 57.17
13	79.7.10	J005940.44-073347.9	0.243	15.838 (± 0.068)	15.163 (± 0.136)	>11.97	>8.677	00 59 40.444	-07 33 47.97
16	79.7.13	J005948.05-073806.6	1.603	12.231 (± 0.024)	12.246 (± 0.028)	>11.296	>8.047	00 59 48.059	-07 38 06.64
17	79.7.14	J005954.59-073656.3	0.621	16.560 (± 0.112)	15.736 (± 0.208)	11.916 (± 0.374)	>8.813	00 59 54.590	-07 36 56.34
19	79.7.16	J010007.40-073521.9	0.799	16.751 (± 0.129)	15.577 (± 0.187)	>11.541	>8.065	01 00 07.400	-07 35 21.97
20	79.7.17	J005956.49-073832.0	1.054	15.665 (± 0.057)	14.760 (± 0.102)	11.776 (± 0.330)	>8.81	00 59 56.500	-07 38 32.03
24	80.6.03	J183400.84+492029.5	1.144	17.119 (± 0.096)	15.528 (± 0.081)	12.354 (± 0.216)	>9.468	18 34 00.841	+49 20 29.50
27	80.6.06	J183412.30+492154.6	1.496	16.195 (± 0.052)	15.359 (± 0.071)	13.309 (± 0.503)	>9.164	18 34 12.302	+49 21 54.60
31	80.7.01	J183402.16+491816.9	0.166	15.489 (± 0.038)	14.660 (± 0.046)	>12.574	9.471 (± 0.416)	18 34 02.163	+49 18 17.00
35	80.7.05	J183333.40+491617.2	0.189	15.778 (± 0.041)	14.790 (± 0.047)	12.659 (± 0.341)	9.295 (± 0.373)	18 33 33.402	+49 16 17.28
36	80.7.06	J183416.40+491544.3	0.196	14.553 (± 0.029)	13.181 (± 0.027)	10.253 (± 0.043)	7.746 (± 0.094)	18 34 16.404	+49 15 44.30
39	80.7.09	J183346.08+491711.1	0.479	11.416 (± 0.024)	11.429 (± 0.021)	11.742 (± 0.130)	>9.66	18 33 46.088	+49 17 11.19
40	80.7.10	J183415.71+491242.0	0.462	15.494 (± 0.038)	14.844 (± 0.051)	12.050 (± 0.176)	9.080 (± 0.320)	18 34 15.713	+49 12 42.06
43	80.7.13	J183327.02+491737.2	0.854	16.364 (± 0.056)	16.072 (± 0.118)	>13.219	>9.725	18 33 27.027	+49 17 37.25
44	80.7.14	J183331.78+491417.0	0.919	7.570 (± 0.025)	7.664 (± 0.020)	7.596 (± 0.017)	7.644 (± 0.083)	18 33 31.787	+49 14 17.03
48	81.6.02	J010509.05-060648.7	1.090	16.228 (± 0.068)	14.796 (± 0.076)	>12.471	>9.126	01 05 09.052	-06 06 48.71
51	81.6.05	J010442.21-060710.5	1.318	15.435 (± 0.044)	13.841 (± 0.044)	10.824 (± 0.136)	8.394 (± 0.270)	01 04 42.216	-06 07 10.56
55	81.7.04	J010502.62-061508.9	0.172	16.294 (± 0.072)	15.316 (± 0.122)	>12.592	>8.96	01 05 02.622	-06 15 08.92

TABLE 6
CONTINUED

N (1)	Source Name (2)	Identification (WISE) (3)	Δ ($''$) (4)	W1 (mag) (5)	W2 (mag) (6)	W3 (mag) (7)	W4 (mag) (8)	R.A. (WISE) (9)	Decl. (WISE) (10)
58	81.7.08	J010516.06–061747.9	0.680	16.279 (± 0.069)	15.404 (± 0.128)	>11.867	>9.251	01 05 16.062	–06 17 47.98
59	81.7.09	J010500.17–061540.4	0.167	17.193 (± 0.143)	16.061 (± 0.206)	>12.589	>9.284	01 05 00.177	–06 15 40.48
62	81.7.12	J010515.54–061640.2	1.202	16.474 (± 0.079)	15.746 (± 0.165)	12.295 (± 0.397)	>8.862	01 05 15.546	–06 16 40.29
64	81.7.14	J010517.06–061825.1	0.938	17.810 (± 0.245)	15.711 (± 0.158)	12.568 (± 0.529)	>8.548	01 05 17.063	–06 18 25.15
67	81.8.01	J010529.68–061733.4	0.629	17.052 (± 0.137)	16.000 (± 0.225)	12.240 (± 0.402)	>8.813	01 05 29.680	–06 17 33.49
69	81.8.03	J010513.11–062152.3	1.678	16.444 (± 0.082)	15.648 (± 0.165)	>12.178	>9.081	01 05 13.116	–06 21 52.30
73	82.6.04	J153731.62+060316.0	0.142	17.175 (± 0.173)	15.833 (± 0.183)	>12.771	>8.659	15 37 31.621	+06 03 16.09
74	82.6.05	J153724.64+060102.9	0.326	17.298 (± 0.198)	16.810 (± 0.459)	12.542 (± 0.438)	>8.794	15 37 24.644	+06 01 02.94
75	82.6.06	J153715.39+055906.7	1.367	15.386 (± 0.047)	14.393 (± 0.058)	12.371 (± 0.373)	9.096 (± 0.524)	15 37 15.391	+05 59 06.72
78	82.6.09	J153725.29+060330.5	1.494	16.553 (± 0.101)	16.268 (± 0.268)	>12.378	>9.205	15 37 25.300	+06 03 30.59
79	82.6.10	J153712.46+060053.8	0.627	15.982 (± 0.067)	16.272 (± 0.289)	12.267 (± 0.356)	9.072 (± 0.531)	15 37 12.464	+06 00 53.86
80	82.6.11	J153708.16+060549.8	0.473	16.011 (± 0.070)	15.145 (± 0.100)	12.080 (± 0.279)	>8.653	15 37 08.165	+06 05 49.80
93	82.8.02	J153758.31+054724.3	1.649	10.371 (± 0.024)	10.193 (± 0.021)	10.077 (± 0.050)	>8.928	15 37 58.316	+05 47 24.32
94	83.6.01	J112646.16+534922.4	1.075	16.549 (± 0.091)	15.280 (± 0.102)	12.374 (± 0.309)	>8.901	11 26 46.170	+53 49 22.42
97	83.6.05	J112629.27+535007.5	1.529	16.310 (± 0.077)	15.936 (± 0.169)	>12.511	>9.314	11 26 29.279	+53 50 07.58
101	83.7.01	J112656.12+533933.0	0.892	17.402 (± 0.180)	16.457 (± 0.277)	12.420 (± 0.328)	>9.001	11 26 56.127	+53 39 33.06
102	83.7.02	J112659.30+534518.0	1.620	17.434 (± 0.194)	16.801 (± 0.369)	>12.839	>8.789	11 26 59.310	+53 45 18.10
103	83.7.03	J112642.18+534258.7	0.290	7.768 (± 0.024)	7.844 (± 0.020)	7.807 (± 0.017)	7.648 (± 0.131)	11 26 42.189	+53 42 58.76
108	83.7.08	J112645.61+533910.8	0.274	16.831 (± 0.111)	15.384 (± 0.107)	12.529 (± 0.352)	8.845 (± 0.330)	11 26 45.619	+53 39 10.85
112	84.6.03	J092036.99+641348.7	0.589	16.997 (± 0.147)	16.129 (± 0.224)	12.501 (± 0.370)	>8.684	09 20 36.993	+64 13 48.75
124	84.7.12	J092032.13+640423.1	0.593	15.582 (± 0.048)	14.879 (± 0.072)	11.205 (± 0.105)	8.606 (± 0.288)	09 20 32.138	+64 04 23.16
126	84.7.14	J092011.18+640723.7	0.503	13.735 (± 0.026)	13.679 (± 0.037)	12.898 (± 0.512)	>8.848	09 20 11.183	+64 07 23.77
127	84.7.15	J091947.69+640743.5	0.345	16.339 (± 0.079)	16.842 (± 0.420)	>12.546	>9.352	09 19 47.699	+64 07 43.57
129	84.7.18	J092043.53+640050.2	1.401	17.210 (± 0.162)	15.468 (± 0.126)	>12.925	>8.846	09 20 43.537	+64 00 50.26
131	84.8.01	J091947.14+635716.0	1.801	15.958 (± 0.064)	14.781 (± 0.070)	>12.354	>8.871	09 19 47.140	+63 57 16.06
132	84.8.02	J092037.62+635827.7	0.560	17.168 (± 0.145)	16.001 (± 0.189)	12.519 (± 0.348)	>9.162	09 20 37.627	+63 58 27.76
133	84.8.03	J091955.38+635934.2	0.201	16.905 (± 0.127)	15.669 (± 0.138)	>13.004	>9.3	09 19 55.388	+63 59 34.21
134	84.8.04	J092004.99+635526.3	1.693	15.869 (± 0.054)	14.958 (± 0.079)	>12.175	>9.321	09 20 04.992	+63 55 26.33
136	85.6.01	J103535.27–244318.3	1.068	15.665 (± 0.056)	14.297 (± 0.051)	11.716 (± 0.180)	>8.653	10 35 35.276	–24 43 18.39
137	85.6.02	J103510.44–243845.9	0.827	15.969 (± 0.064)	14.860 (± 0.080)	12.170 (± 0.290)	>8.387	10 35 10.442	–24 38 45.96
138	85.6.03	J103514.50–243940.7	1.711	16.281 (± 0.081)	15.544 (± 0.141)	12.125 (± 0.271)	>8.653	10 35 14.506	–24 39 40.73
144	85.7.05	J103522.79–244631.6	0.163	12.084 (± 0.024)	12.132 (± 0.024)	12.087 (± 0.255)	9.191 (± 0.511)	10 35 22.795	–24 46 31.60
153	85.8.03	J103528.09–245346.9	0.489	16.344 (± 0.091)	15.278 (± 0.119)	12.104 (± 0.297)	>8.306	10 35 28.096	–24 53 46.96
154	86.6.02	J114109.70+561523.3	1.261	16.792 (± 0.120)	15.600 (± 0.143)	12.614 (± 0.403)	8.990 (± 0.467)	11 41 09.708	+56 15 23.30
158	86.6.06	J114050.22+561708.0	0.101	16.235 (± 0.080)	15.427 (± 0.123)	12.857 (± 0.497)	>8.657	11 40 50.228	+56 17 08.09
159	86.7.01	J114053.57+561012.6	1.500	16.808 (± 0.117)	16.122 (± 0.224)	>12.893	>9.291	11 40 53.573	+56 10 12.65
160	86.7.02	J114047.64+561059.6	0.678	15.959 (± 0.062)	15.904 (± 0.187)	>12.259	>9.267	11 40 47.643	+56 10 59.64
161	86.7.04	J114038.09+561023.5	0.557	17.085 (± 0.146)	16.198 (± 0.227)	>12.962	>9.253	11 40 38.091	+56 10 23.55
163	86.7.06	J114112.36+561441.0	0.165	16.972 (± 0.131)	15.865 (± 0.178)	>12.541	>9.286	11 41 12.370	+56 14 41.04
164	86.7.07	J114109.69+560818.9	0.194	14.134 (± 0.029)	13.999 (± 0.046)	>12.603	>9.284	11 41 09.699	+56 08 18.99
172	86.8.01	J114124.30+560449.2	0.094	17.177 (± 0.165)	15.625 (± 0.155)	>12.894	>9.352	11 41 24.308	+56 04 49.30
173	86.8.02	J114049.16+560101.5	1.116	17.097 (± 0.140)	15.666 (± 0.133)	>13.012	>9.379	11 40 49.168	+56 01 01.53

NOTE. — Column 1: Source number from Table 4. Column 2: Observation ID, CCD chip number, and WAVDETECT source number. Column 3: Identification number for the identified WISE source. Column 4: Offset between centroid of *Chandra* and WISE sources. Columns 5–8: W1, W2, W3 and W4 WISE magnitudes respectively, with errors. A $>$ implies a magnitude lower limit. Columns 9–10: R.A. and Decl. of the WISE source, in the J2000 epoch.

TABLE 7
SOURCES IN THE SAMPLE GALAXIES

Source Name (1)	N (2)	<i>Chandra</i> ID (CXOU) (3)	D (") (4)	Net Counts (5)	Net Soft (6)	Net Hard (7)	Hardness Ratio (8)	Γ (9)	Unabs. Flux (10)	Inferred L_X (11)	H α ? (12)	Notes (13)
NGC 337 X-1	5	J005952.3–073447	33	43.8 ± 6.7	32.3 ± 5.7	11.5 ± 3.5	-0.47 ± 0.14	$1.77^{+0.35}_{-0.30}$	4.52 ± 0.69	23.2 ± 3.5	Y	ULX
NGC 337 X-2	6	J005951.9–073458	32	14.0 ± 3.9	4.5 ± 2.2	9.5 ± 3.2	0.36 ± 0.26	$0.13^{+0.50}_{-0.13}$	1.44 ± 0.40	7.40 ± 2.05	Y	
NGC 337 X-3	7	J005950.6–073458	19	315.4 ± 17.8	194.8 ± 14.0	120.6 ± 11.0	-0.24 ± 0.05	$1.26^{+0.11}_{-0.11}$	32.5 ± 1.8	167 ± 9	Y	ULX
NGC 337 X-4	8	J005950.4–073454	14	43.2 ± 6.7	26.7 ± 5.3	16.5 ± 4.1	-0.24 ± 0.15	$1.26^{+0.31}_{-0.29}$	4.46 ± 0.69	22.9 ± 3.6	Y	ULX
NGC 337 X-5	9	J005949.5–073523	44	24.8 ± 5.0	18.0 ± 4.2	6.9 ± 2.6	-0.45 ± 0.18	$1.70^{+0.45}_{-0.38}$	2.56 ± 0.52	13.1 ± 2.6	Y	ULX (c)
NGC 337 X-6	10	J005949.5–073436	10	109.3 ± 10.5	64.7 ± 8.1	44.7 ± 6.7	-0.18 ± 0.09	$1.16^{+0.18}_{-0.18}$	11.3 ± 1.1	57.8 ± 5.6	..	ULX
NGC 337 X-7	11	J005948.5–073457	28	61.5 ± 7.9	41.7 ± 6.5	19.8 ± 4.5	-0.36 ± 0.12	$1.50^{+0.27}_{-0.24}$	6.34 ± 0.81	32.5 ± 4.2	Y	ULX (b)
NGC 337 X-8	12	J005947.5–073417	45	45.2 ± 6.8	41.7 ± 6.5	3.5 ± 2.0	-0.85 ± 0.08	$3.05^{+0.69}_{-0.42}$	4.66 ± 0.70	23.9 ± 3.6	Y	ULX (a,c)
NGC 337 X-9	14	J005953.3–073521	62	25.4 ± 5.1	14.5 ± 3.9	11.0 ± 3.3	-0.14 ± 0.20	$1.07^{+0.39}_{-0.37}$	2.62 ± 0.53	13.5 ± 2.7	Y	ULX (a)
NGC 337 X-10	15	J005953.3–073457	51	4.4 ± 2.2	2.7 ± 1.7	1.7 ± 1.4	-0.23 ± 0.50	$1.24^{+1.23}_{-0.92}$	0.45 ± 0.23	2.32 ± 1.19	..	
IC 1291 X-1	32	J183355.8+491746	71	72.8 ± 8.5	33.9 ± 5.8	38.9 ± 6.2	0.07 ± 0.12	$0.66^{+0.21}_{-0.22}$	7.25 ± 0.85	86.1 ± 10.1	..	(a)
IC 1291 X-2	33	J183351.5+491642	11	28.5 ± 5.4	25.7 ± 5.1	2.8 ± 1.7	-0.80 ± 0.11	$2.77^{+0.76}_{-0.45}$	2.84 ± 0.54	33.8 ± 6.4	Y	ULX
IC 1291 X-3	37	J183350.6+491558	49	10.6 ± 3.3	8.8 ± 3.0	1.8 ± 1.4	-0.66 ± 0.24	$2.22^{+1.16}_{-0.62}$	1.05 ± 0.33	12.5 ± 3.9	..	
IC 1291 X-4	38	J183355.5+491741	64	8.7 ± 3.0	5.8 ± 2.5	2.9 ± 1.7	-0.33 ± 0.32	$1.42^{+0.79}_{-0.62}$	0.86 ± 0.30	10.2 ± 3.6	Y	(a)
PGC 3853 X-1	52	J010511.3–061207	103	182.6 ± 13.5	130.8 ± 11.4	51.8 ± 7.2	-0.43 ± 0.07	$1.62^{+0.15}_{-0.14}$	18.2 ± 1.4	28.4 ± 2.1	..	ULX
PGC 3853 X-2	57	J010504.5–061323	39	4.6 ± 2.2	4.8 ± 2.2	-0.2 ± 0.1	-1.09 ± 0.06	..	0.46 ± 0.22	0.71 ± 0.35	..	
PGC 3853 X-3	66	J010505.3–061148	57	4.8 ± 2.2	3.0 ± 1.7	1.8 ± 1.4	-0.25 ± 0.45	$1.24^{+1.10}_{-0.83}$	0.48 ± 0.22	0.75 ± 0.35	..	
NGC 5964 X-1	81	J153738.9+055845	44	39.3 ± 6.3	26.6 ± 5.2	12.7 ± 3.6	-0.35 ± 0.15	$1.43^{+0.34}_{-0.29}$	3.82 ± 0.61	27.9 ± 4.5	..	ULX
NGC 5964 X-2	83	J153733.1+055756	55	23.5 ± 4.9	16.8 ± 4.1	6.7 ± 2.6	-0.43 ± 0.19	$1.59^{+0.47}_{-0.38}$	2.28 ± 0.48	16.6 ± 3.5	..	ULX
NGC 5964 X-3	85	J153733.4+055915	68	10.4 ± 3.3	7.7 ± 2.8	2.8 ± 1.7	-0.47 ± 0.28	$1.68^{+0.79}_{-0.57}$	1.01 ± 0.32	7.40 ± 2.36	Y	(a)
NGC 5964 X-4	92	J153730.8+055852	86	4.9 ± 2.2	1.0 ± 1.0	4.0 ± 2.0	0.60 ± 0.36	..	0.48 ± 0.22	3.48 ± 1.59	..	
UGC 6446 X-1	104	J112635.7+534456	43	4.7 ± 2.2	3.8 ± 2.0	1.0 ± 1.0	-0.58 ± 0.37	$1.88^{+1.97}_{-0.80}$	0.43 ± 0.20	1.65 ± 0.78	..	
NGC 2805 X-1	113	J092020.6+640607	3	4.6 ± 2.2	3.9 ± 2.0	0.8 ± 1.0	-0.66 ± 0.38	$2.18^{+1.82}_{-0.91}$	0.46 ± 0.22	4.30 ± 2.10	Y	
NGC 2805 X-2	114	J092019.5+640454	76	37.4 ± 6.2	21.8 ± 4.7	15.7 ± 4.0	-0.16 ± 0.16	$1.06^{+0.31}_{-0.30}$	3.73 ± 0.61	35.0 ± 5.8	Y	(a)
NGC 2805 X-3	115	J092013.7+640606	44	95.7 ± 9.8	62.9 ± 7.9	32.8 ± 5.7	-0.31 ± 0.10	$1.35^{+0.20}_{-0.19}$	9.54 ± 0.98	89.5 ± 9.2	Y	ULX (a,c)
NGC 2805 X-4	116	J092006.3+640738	128	102.8 ± 10.1	79.0 ± 8.9	23.9 ± 4.9	-0.54 ± 0.08	$1.83^{+0.23}_{-0.19}$	10.2 ± 1.0	96.2 ± 9.5	Y	ULX
NGC 2805 X-5	117	J092021.0+640617	8	6.6 ± 2.6	3.8 ± 2.0	2.8 ± 1.7	-0.15 ± 0.39	$1.04^{+0.82}_{-0.73}$	0.66 ± 0.26	6.22 ± 2.48	Y	
NGC 2805 X-6	118	J092019.5+640624	15	8.6 ± 3.0	6.8 ± 2.6	1.8 ± 1.4	-0.58 ± 0.29	$1.95^{+1.13}_{-0.64}$	0.86 ± 0.30	8.04 ± 2.81	Y	(c)
NGC 2805 X-7	119	J092018.6+640615	13	12.5 ± 3.6	6.9 ± 2.6	5.7 ± 2.5	-0.10 ± 0.29	$0.93^{+0.55}_{-0.52}$	1.25 ± 0.36	11.7 ± 3.4	Y	(c)
NGC 2805 X-8	120	J092014.9+640436	101	24.6 ± 5.0	18.8 ± 4.4	5.9 ± 2.5	-0.52 ± 0.18	$1.80^{+0.50}_{-0.39}$	2.46 ± 0.50	23.0 ± 4.7	Y	ULX

TABLE 7
 CONTINUED

Source Name (1)	N (2)	<i>Chandra</i> ID (CXOU) (3)	D ('') (4)	Net Counts (5)	Net Soft (6)	Net Hard (7)	Hardness Ratio (8)	Γ (9)	Unabs. Flux (10)	Inferred L_X (11)	H α ? (12)	Notes (13)
NGC 2805 X-9	121	J092013.1+640440	102	7.7 ± 2.8	6.9 ± 2.6	0.9 ± 1.0	-0.77 ± 0.24	$2.57^{+1.43}_{-0.75}$	0.77 ± 0.28	7.22 ± 2.65	Y	(a)
NGC 2805 X-10	122	J092034.5+640643	98	5.5 ± 2.5	4.8 ± 2.2	0.7 ± 1.0	-0.75 ± 0.33	$2.47^{+1.53}_{-0.92}$	0.55 ± 0.25	5.12 ± 2.30	Y	(a)
NGC 2805 X-11	123	J092033.2+640345	168	8.6 ± 3.0	6.7 ± 2.6	1.9 ± 1.4	-0.56 ± 0.29	$1.89^{+1.05}_{-0.63}$	0.86 ± 0.30	8.06 ± 2.81	...	
NGC 2805 X-12	124	J092032.1+640424	131	9.7 ± 3.2	4.9 ± 2.2	4.8 ± 2.2	-0.01 ± 0.32	$0.78^{+0.60}_{-0.60}$	0.96 ± 0.32	9.04 ± 2.96	Y	(b,c)
NGC 2805 X-13	125	J092020.2+640409	121	4.5 ± 2.2	1.7 ± 1.4	2.8 ± 1.7	0.24 ± 0.48	$0.31^{+0.88}_{-0.31}$	0.45 ± 0.22	4.19 ± 2.10	...	
NGC 2805 X-14	126	J092011.2+640723	168	9.6 ± 3.2	8.8 ± 3.0	0.8 ± 1.0	-0.83 ± 0.20	$2.87^{+1.13}_{-0.77}$	0.96 ± 0.32	9.00 ± 2.96	...	Star (a,b,c)
ESO 501-23 X-1	141	J103522.2-244513	14	867.0 ± 29.5	528.7 ± 23.0	338.3 ± 18.4	-0.22 ± 0.03	$1.17^{+0.07}_{-0.06}$	84.7 ± 2.9	49.8 ± 1.7	Y	ULX
ESO 501-23 X-2	142	J103523.3-244517	2.2	68.3 ± 8.3	40.7 ± 6.4	27.6 ± 5.3	-0.19 ± 0.12	$1.12^{+0.23}_{-0.22}$	6.67 ± 0.81	3.92 ± 0.48	Y	(a)
ESO 501-23 X-3	144	J103522.8-244632	77	8.5 ± 3.0	8.8 ± 3.0	-0.3 ± 0.1	-1.07 ± 0.03	...	0.83 ± 0.29	0.49 ± 0.17	...	Star (a,b)
ESO 501-23 X-4	145	J103522.6-244503	14	17.7 ± 4.4	11.5 ± 3.5	6.2 ± 2.7	-0.30 ± 0.24	$1.33^{+0.53}_{-0.46}$	1.73 ± 0.43	1.02 ± 0.25	...	

NOTE. — Column 1: Source name. Column 2: Source number from Table 4. Column 3: *Chandra* ID name. Column 4: Projected distance from galactic nucleus. Columns 5, 6, 7: Net broad, soft, and hard detected counts within 2.3'' aperture, respectively. Column 8: Hardness Ratio, defined as $(H-S)/(H+S)$ where H is hard counts and S is soft counts, with Gaussian errors. These are calculated using background subtracted count values, so they may not precisely map to other values in this table. Column 9: Approximate value of the power law exponent (Γ) that would produce the observed ratio of hard to soft counts. Column 10: Unabsorbed flux in units of $10^{-14} \text{ erg s}^{-1} \text{ cm}^{-2}$, calculated in PIMMS with a $\Gamma=1.7$ power law, including galactic absorption. Source counts were extracted from the 0.3-8 keV band, and extrapolated to 0.3-10 keV. Column 11: Inferred luminosity of the source, at the galactic distance, in units of $10^{38} \text{ erg s}^{-1}$. This is only valid for sources that are in fact associated with the galaxy. Column 12: Does this object coincide with H α emission from MDM imaging? Column 13: ULX indicates a ULX candidate. (a) indicates a match in the UNSO-B1.0 catalog, (b) indicates a match in the WISE point source catalog, and (c) indicates a match in the SDSS DR8 catalog.